UHMET 88-02

EQUATORWARD SURGES, EQUATORIAL WESTERLIES AND CONVECTION ON INTERANNUAL AND INTRASEASONAL TIME SCALES

by Takio Murakami and
Waduwawatte Sumathipala

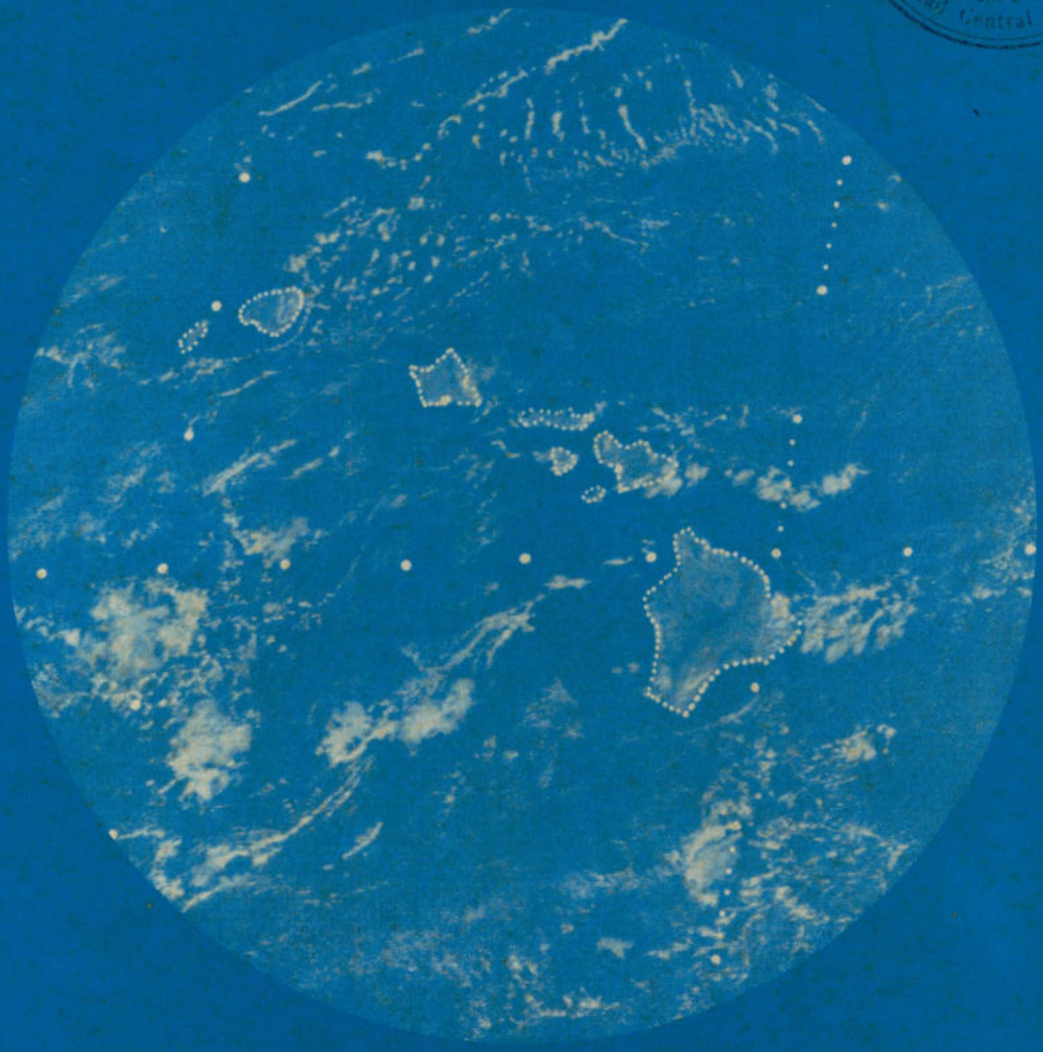

Supported by
National Science Foundation, Washington, D.C.
under Grant No. ATM-8609968

November 1988

Department of Meteorology, University of Hawaii

UHMET88-02

Equatorward Surges, Equatorial Westerlies and Convection on Interannual and Intraseasonal Time Scales[1]

by

Takio Murakami and Waduwawatte L. Sumathipala[2]

Department of Meteorology
University of Hawaii

Supported by
National Science Foundation, Washington, D. C.
Under Grant No. ATM-8609968

November 1988

---

[1] Report No. UHMET88-02, Department of Meteorology, University of Hawaii, Honolulu, Hawaii

[2] Present affiliation: State University of New York, College at Oswego, Oswego, New York

Table of Contents

ABSTRACT

Based on 850 mb (u, v) wind and outgoing longwave radiation (OLR) data during the six years of 1980-85, ENSO modes are described in terms of three-month running mean anomalies which are denoted as u", v", and OLR", respectively. Daily (u, v, OLR) data are grouped into three frequency bands, i.e., L-mode (30-60 day filtered u_L, v_L, and OLR_L); M-mode (7-20 day filtered u_M, v_M, and OLR_M); and S-mode (1-6 day filtered u_S, v_S, and OLR_S).

Atmospheric ENSO modes are characterized by typical spatial scales of zonal wavenumbers 1 and 2, and a very slow eastward phase speed of about 0.3 m s^{-1}, taking more than 2 years to travel from their birthplace in the Indian Ocean to the eastern Pacific. These ENSO modes weaken considerably while passing over the maritime continent (Sumatra, Borneo, and New Guinea), followed by an anomalous intensification when they arrive in the central Pacific. At any fixed geographical location, the ENSO onset is associated with the eastward propagation of u">0 (westerly) and OLR"<0 (wet) perturbations. Likewise, the eastward propagation of u"<0 (easterly) and OLR">0 (dry) perturbations is important in determining the ENSO withdrawal. Transient westerly and/or easterly bursts occurring over regions far upstream appear to contribute little to the phase changes of ENSO modes.

L-modes over the Indian Ocean during southern winter and the western Pacific during northern winter exhibit a symmetric character with respect to the equator. The longitudinal extent of equatorial westerlies, which may serve as the energy source for oceanic Kelvin waves, amounts to about 80°, being much smaller than the corresponding scale (120°) of ENSO modes. Over the South China Sea, wintertime cold v_L surges do not enhance equatorial westerlies and convection on 30-60 day time scales. M-mode is not an equatorially trapped mode and shows an asymmetric character with respect to the equator. During northern winter, the western north Pacific is characterized by a prominent N-S extended trough,

exemplifying a possible midlatitude-tropical interaction on 7-20 day time scales. Northerly v_M surges over the South China Sea do not induce significant westerlies along the equator; however, these strong surges do lead to cross-equatorial flows, and to the enhancement of monsoonal westerlies and rains over Indonesia. The longitudinal extent of u_M westerlies along the equator is small, amounting only to about 30°. The most noteworthy feature of S-mode is the dominance of the meridional over the zonal component of the winds. Thus, equatorward v_S surges do not effectively enhance westerlies along the equator.

L-modes propagate systematically eastward (5 to 6 m s^{-1}) across the equatorial Indian Ocean and the western Pacific, while M-modes generally propagate westward with an average phase speed of 9 m s^{-1}. The phase propagation of S-modes is not as well defined as L- and M-modes. The Indian Ocean near 80°E and the western Pacific around 140°E are two of the most favorable regions for the occurrence of strong u_L, u_M, and u_S westerly (or easterly) bursts.

The changes in activity of u_L, u_M, and u_S zonal wind bursts on the interannual time scale are expressed in terms of 3-month running mean anomaly eddy kinetic energy, i.e., K''_L, K''_M, and K''_S, respectively. The simultaneous (no lag) correlation between u" and K''_L exceeds the 95% confidence level over the western Pacific between about 140°E and the date line, perhaps indicating an in situ nonlinear coupling between interannual u" modes and groups (not individual) of intraseasonal L-modes over the same region. Of particular interest is a large positive correlation between u" and K''_M in excess of +0.45 over the eastern Pacific (180°-120°W) at lag -10 to -2 months (K''_M leading). Thus, an ensemble effect of M-modes may contribute to the in situ development of interannual ENSO modes over the eastern Pacific. The contribution due to groups of S-modes appears to be less significant.

1. Introduction

This paper is a sequel to the recent paper by Murakami and Sumathipala (1988) which investigated the nature of equatorial westerly bursts before, during, and after the 1982/83 ENSO.[3] The reader is directed to their paper (hereafter referred to as MS) for a detailed description of westerly bursts, as only a brief outline will be presented here. In MS some of the characteristic features of the ENSO were described in terms of three-month running mean anomalies, which were signified as u", v", OLR", and SST", respectively. Daily 850 mb winds and OLR data were subjected to a band-pass filter to obtain climatological information on atmospheric "westerly bursts." These filtered data were denoted as u_S, v_S, and OLR_S (1-6 day); u_M, v_M, and OLR_M (7-20 day); and u_L, v_L, OLR_L (30-60 day); respectively. Thus, these intraseasonal perturbations are clearly separate from interannual ENSO modes whose time scales are longer than three months.

Atmospheric interannual u" and OLR" modes are characterized by typical spatial scales of zonal wavenumbers 1 and 2, and very slow eastward phase propagations of about 0.3 m s^{-1} all the way from the western Indian Ocean to the eastern Pacific. Oceanic interannual SST" modes also exhibit a slow eastward movement across the Pacific. It has been customary to define the ENSO onset as occurring over the central and eastern equatorial Pacific. However, it is possible to define the ENSO onset at any location by phase changes from easterly (u"<0) to westerly (u">0) anomalies, and from below normal (OLR">0) to above normal (OLR"<0) convective activity. Therefore, the timing of the ENSO onset may differ significantly from one geographic location to another.[4]

---

[3] A list of acronyms and symbols is given in the Appendix.

[4] This is analogous to the monsoon onset over South Asia. In association with the northward migration of the intertropical convergence zone, the monsoon begins first over the Malaysian Peninsula in late April, followed by the monsoon onset over south India and Indochina sometime in May. The monsoon over central

Rasmusson and Carpenter (1982) and Holland (1986) showed that there is a tendency for convection and westerly wind anomalies over the Indonesian-northern Australian region to precede the ENSO onset over the equatorial eastern Pacific by almost one year or even longer. This is consistent with the slow (0.3 m s^{-1}) eastward propagation of ENSO modes. The birthplace of ENSO modes appears to be the western end of the Indian Ocean (Barnett, 1983; Yasunari, 1987; Meehl, 1987). ENSO modes weaken considerably while passing over the maritime continent (Sumatra, Borneo, New Guinea), followed by an anomalous intensification when they reach the central Pacific. Moreover, the eastward propagation of anomalous easterlies (u"<0) and below normal convection (OLR">0) across the Indian Ocean, the maritime continent, and the Pacific Ocean is equally important. This easterly and dry phase is associated with the initiation of an anti-ENSO phase over these regions. Meehl (1987) and Yasunari (1988) demonstrated the biennial nature of the eastward propagating interannual signal which involves a modulation of the annual cycle. Based on an atmosphere-ocean coupled model, Yamagata (1988) showed that his numerically simulated perturbations exhibit characteristics analogous to those of observed ENSO modes with an eastward phase speed of about 0.6 m s^{-1}. Similar results were also obtained by Lau and Shen (1988). No external forcings were prescribed in their models, thus these perturbations can be identified as a free atmosphere-ocean coupled mode.

Barnett (1977, 1981) and Lukas et al. (1984) suggested a scenario in which an El Nino over the eastern Pacific is triggered (or forced) by equatorial westerly wind bursts occurring over the western Pacific. These westerly bursts are thought to be responsible for the excitation of oceanic Kelvin waves that propagate very quickly (about 2 to 3 m s^{-1}) eastward across the central Pacific, reaching the eastern end about three months later

---

India does not commence until mid-June.

where they then induce the onset of an El Nino event (Wyrtki, 1975). In other words, the phase speed of oceanic Kelvin waves, which can be regarded as a forced mode, is about ten times faster than the corresponding speed of the interannual ENSO modes. The westerly burst concept has triggered many investigations that focused on observationally confirming the existence of westerly bursts (e.g., Keen, 1982; Luther et al., 1983; Lukas et al., 1984). In addition, many modelers have attempted to simulate the oceanic response to westerly bursts (e.g., McCreary, 1983; Eriksen et al., 1983; Harrison and Schopf, 1984). Despite the efforts of these synoptic and model investigators, many problems still remain unsolved. First of all, exact time and space scales of westerly bursts have never been clearly defined. Harrison (1987) utilized monthly mean surface wind data for describing the nature of westerly bursts over the central Pacific. However, transient wind variations with periods shorter than 30 days are almost entirely eliminated from the monthly mean data, although the residuals of 30-60 day oscillations are still present. Namely, the monthly mean wind data largely reflect the interannual wind variations associated with ENSO modes, and thus they are not appropriate for describing the evolution of transient westerly bursts. Monthly mean data also inhibit the investigation of fast moving oceanic Kelvin waves and their associated atmospheric perturbations. Monthly mean wind and/or SST analyses have been widely used as forcing fields for hindcast El Nino events via pure ocean circulation models (e.g., Busalacchi and O'Brien, 1981; Harrison and Schopf, 1984). Here the initial conditions they applied, primarily reflect the interannual ENSO perturbations themselves, rather than the westerly bursts of the western Pacific. Thus the models predict the oceanic response over the central and eastern Pacific to eastward propagating atmospheric ENSO modes which have already traveled through the Indian Ocean and the maritime continent, and have just reached the western Pacific; therefore these responses may not necessarily support the westerly burst

concept. It is highly probable that oceanic Kelvin waves could be excited due to an imbalance between the prescribed initial conditions and the dynamics inherent to each proposed oceanic model. Efforts should be made to minimize (or completely eliminate) unwanted fast-moving noises during the first phase of numerical experimentation. Nonetheless, the most pressing need is for a unified and detailed definition of westerly bursts; in particular, their time and space scales, which can serve as an acceptable observational basis when utilizing oceanic models for testing the westerly burst concept.

In MS westerly bursts were categorized into 3 intraseasonal frequency bands, i.e., (u_L, u_M, u_S). Hence their time scales are clearly defined, and they do not include any interannual u" components. An attempt was then made to determine the space structural characteristics of intraseasonal (u_L, u_M, u_S) westerly bursts by means of compositing techniques. Westerly u_L bursts are sandwiched between twin cyclonic disturbances which are nearly symmetric with respect to the equator. The east-west extent of u_L westerlies along the equator is about 9,000 km, while the corresponding extent of u_M westerlies amounts to about 4,000 km. The (u_M, v_M) wind field is asymmetric with respect to the equator and is characterized by cold equatorward surges from the winter hemisphere midlatitude region. The longitudinal scale of u_S westerlies along the equator is only 2,000 km or less. Thus, the structure of westerly bursts varies significantly with different periodicities. Furthermore westerly bursts are not unique to the western Pacific, rather they are also prominent over the central Indian Ocean.

MS also investigated the relationship between synoptic-scale westerly bursts on time scales of a few days and the planetary-scale interannual modes by counting the number of days of westerlies in each season at every 20 degrees of longitude from 40°E to 100°W along the equator. It appears that the number of days of westerlies is not an appropriate index for describing the

activity of westerly bursts. After the ENSO onset, the westerly phase of interannual u" variations is associated with persistent westerly winds day after day for an extended period which is longer than a season. The immediate consequence is a large number of days of westerlies for that particular season. Therefore, the large number of days of westerlies reflects the westerly phase of interannual u" variations, and does not necessarily indicate the frequent occurrence of westerly bursts. Because of the difference in time and space scales, there exists no direct correlation between westerly bursts and the interannual ENSO modes. However, it may be possible that groups of transient westerly bursts can interact with interannual modes. This possibility was examined in MS by evaluating the standard deviation of u_L, u_M, and u_S, which is proportional to kinetic energy for each transient mode. These standard deviation fields exhibit the same time and space scales as noted for interannual u" modes. These points will be elaborated on further in Section 6 of the current study.

One of the primary objectives of this study is to investigate the association of equatorial westerlies and convection with equatorward surges from the midlatitude regions of both hemispheres on interannual, as well as intraseasonal time scales. Based on linearized shallow-water equations, Lim and Chang (1981) investigated the dynamic response of the tropical atmosphere to midlatitude forcing. They found that the main tropical response takes the form of a Rossby-wave group, which closely resembles the observed northerly surges over the Asiatic monsoon region. The most important indication in their paper is the significance of the midlatitude influence upon exciting an equatorial response. Subsequently, many other investigators have documented this phenomenon. The tropical response is sensitive to the time scale of the midlatitude forcing. Utilizing surface wind data along a ship track from 30^{o}S to 30^{o}N over the western Pacific, Mitchum (1987) found substantial meridional wind fluctuations on interannual time scales, which are consistent with convergence

into regions of anomalous westerlies and convection to the east of the ship track during ENSO events. With respect to intraseasonal time scales, Murakami (1987, 88a) confirmed the presence of strong 30-60 day equatorward surges at 850 mb, which eventually reach the equatorial region where convection and westerlies become more pronounced than usual. Chang and Lau (1982) detailed the relationship between northerly surges (several days) over the South China Sea, the jet stream and the local Hadley circulation over East Asia, and the equatorial Walker circulation over the Indian Ocean and the Pacific. Sections 3 and 4 will be devoted to a further description of equatorward surges and their associated equatorial convection and zonal wind perturbations on interannual, as well as the three intraseasonal time scales mentioned earlier. On the other hand, Section 5 investigates zonal phase propagation and the changes in intensity (amplitude) of (u_L, u_M, u_S) perturbations along the equator from the western end of the Indian Ocean to the eastern Pacific Ocean.

2. Data and Computational Procedures

Outgoing longwave radiation (OLR) and 850 mb wind (u, v) at a 2.5° longitude-latitude resolution over a tropical belt from 40°N to 40°S during the six years of 1980-85 are utilized in this study. Wind data were extracted from the objectively analyzed data set prepared by the European Centre for Medium Range Weather Forecasts (ECMWF), while OLR data were obtained from polar-orbiting satellites. These data as well as the following computational procedures are the same ones applied in MS, however for the convenience of the reader, the symbols and computational procedures will be explained once again. To begin with, the three-month running mean values for OLR, 850 mb u, and 850 mb v

are computed.[5] For example, the three-month running mean u at month i which is signified by $\langle u \rangle_i$, is computed by

$$\langle u \rangle_i = 0.25\bar{u}_{i-1} + 0.5\bar{u}_i + 0.25\bar{u}_{i+1} \quad , (1)$$

where an overbar $(\bar{})_i$ represents the monthly mean value at month i. The normal annual cycle (denoted as u_n) was determined from the monthly mean $\bar{u}$ value for each month of the year over all years. This normal annual cycle was then removed from $\langle u \rangle_i$ to obtain the interannual component (signified as u") as follows:

$$u'' = \langle u \rangle_i - u_n \quad , (2)$$

Thus, u" includes not only interannual variations with periods longer than one year, but also intra-annual perturbations with periods between three months and one year. Similarly, the interannual components v" and OLR" are computed. For brevity, (u", v", OLR") perturbations will hereafter be referred to as ENSO modes.

The daily transient component u' is obtained by removing the 6-year mean and the normal annual cycle from the daily u. A band-pass filter procedure as formulated by M. Murakami (1979) is applied to the transient u' time series, thus further separating the u' data into three frequency bands denoted as u_L (30-60 day), u_M (7-20 day), and u_S (1-6 day) filtered data, respectively. Likewise these groupings are also applied to the transient v' and OLR' values. In this paper, (u_L, v_L, OLR_L) is termed L-mode, (u_M, v_M, OLR_M) denotes M-mode, and (u_S, v_S, OLR_S) is defined as S-mode.

The data quality of ECMWF analyses was tested by comparing the time series of ECMWF 850 mb u data with the corresponding time

---

[5] Hereafter no mention will be made of the 850 mb level, it will be assumed that all references to wind data (u, v) are at this level unless stated otherwise.

series of surface u wind at several island stations. Refer to MS for further information on the data checking.

Our primary objective is to investigate the relationship between ENSO mode and each intraseasonal component; i.e., L-, M-, and S-mode over the tropical region of the Indian and Pacific Oceans (20^{o}N-20^{o}S, 40^{o}E-80^{o}W). The characteristic features of westerly bursts will be described by u_L, u_M, and u_S along the equator. The next section details the nature (onset, phase propagation, and structure) of the ENSO mode. Common features as well as differences in intraseasonal variations (L-, M-, and S-mode) over the Indian and Pacific Oceans will be discussed in Section 4.

3. ENSO modes

Let us first determine the ENSO onset over the eastern equatorial Pacific as it has customarily been done by many investigators. In Fig. 1C for the time series of u" and OLR" at (0^{o}, 140^{o}W), it may be possible to regard the 3-month period of October-December 1982 as the onset phase over the eastern Pacific. During this transition period, u" tends to gradually increase, while OLR" slowly decreases. February 1983 may correspond to the peak period of the ENSO, when u" westerlies reach a maximum and OLR" becomes minimum. Perhaps the ENSO period ends around July 1983; however, it is difficult to identity the termination of ENSO since both u" and OLR" change so slowly. The timing of the ENSO onset differs significantly from one geographical location to another. The onset over the central Pacific (Fig. 1B; 0^{o}, 180^{o}) appears to take place around May 1982, which is 5 months earlier than the commencement of the ENSO onset over the eastern Pacific. The ENSO period at (0^{o}, 180^{o}) covers approximately 14 months from May 1982 to July 1983. Note that the determination of the ENSO period was made from a subjective inspection of the u" and OLR"

time series. In Fig. 1B, both u" and OLR" change amplitude so gradually that a precise determination of the onset and withdrawal is subject to a 1 or 2 month error. At any rate, the time span for the onset is about 2-3 months which is on the same order as the time scale for oceanic Kelvin waves to traverse from the western end to the eastern end of the Pacific Ocean. This point should be kept in mind when considering the role of intraseasonal westerly bursts upon the ENSO onset.

Over the western Pacific, day-to-day u and OLR fluctuations are complicated (not shown). In this region the wind field shows a strong seasonality which is associated with the Indonesian monsoon. As the monsoon trough migrates across the equator, the mean wind direction alternates between east and west. Climatologically, fall and spring transition seasons should have more westerly winds around 140°E where a double trough condition is found. However, it is not easy to pinpoint the ENSO onset and withdrawal from only an inspection of the local time series of u" and OLR", such as was possible in Figs. 1B and C. As will be mentioned later, the ENSO onset and/or withdrawal at any particular geographical location is related to the eastward propagation of the ENSO mode (u", OLR"). This eastward propagating characteristic was considered when determining the onset/withdrawal at 0°, 140°E (Fig. 1A); consequently, the onset over the western Pacific occurs about a half year prior to the ENSO onset at the date line.

Mitchum (1987) claimed that the ENSO onset over the western Pacific was preceded by pronounced equatorward convergence due to v". However in Fig. 1A for 140°E, one does not see any indication of an increase in v" at 15°N and 15°S prior to the ENSO onset. In fact at 15°N, strong northerlies (v"<0) occur during the late ENSO phase, while v" at 15°S exhibits pronounced southerly flows (v">0) after the ENSO withdrawal. For this particular location (140°E), equatorward convergence due to v" does not take place during the early phase of the ENSO mode, but rather during the

late phase of ENSO. The same is true at 180° (Fig. 1B) and 140°W (Fig. 1C). Equatorward convergence is associated with the structure as well as the eastward propagation of the ENSO mode. In order to examine this phenomenon more specifically, let us look at Fig. 2. During the peak ENSO phase (Fig. 2C), strong westerlies cover the eastern Pacific where convective activity is much pronounced than normal. Concurrently, over the western Pacific and maritime continent, prominent easterlies coincide with below normal convective activity. This is indicative of an eastward shift in the equatorial east/west Walker circulation from its normal position near Indonesia to a region centered around 140°W at the peak ENSO phase. Around and slightly to the west of the date line, note the presence of northerly winds over the North Pacific, and southerly winds emanating from the South Pacific midlatitudes (Fig. 2C). Namely, these equatorward convergent flows are most pronounced about 40° of longitude upstream of the strong equatorial westerlies prevailing over the eastern Pacific. This reflects an unusual development of the Hadley circulation (strong equatorward convergence) over the western Pacific during the peak ENSO phase of the eastern Pacific. At any rate, the eastward propagating (u", v") wind system as shown in Fig. 2 resembles the structure of a heat-induced Kelvin wave as discussed by Gill (1980). Refer also to Wang and Murakami (1988) for a detailed description of the (u", v", OLR") ENSO modes.

Barnett (1983), Yasunari (1987), and Meehl (1987) identified the equatorial Indian Ocean as the birthplace of interannual westerly modes. This can be reconfirmed in Fig. 2A which shows the first development of equatorial westerlies over the Indian Ocean. Interestingly, this development occurs more than 1 1/2 years prior to the ENSO onset over the eastern Pacific. These equatorial westerlies slowly immigrate northward from their birthplace in the western Indian Ocean, reaching the Asiatic monsoon region (Arabian Sea, Bay of Bengal, and the South China

Sea) by July 1982 (Fig. 2B). Simultaneously, they arrive in the western Pacific, having propagated eastward with a phase speed of approximately 5-8^{o} longitude per month. This northward as well as eastward propagation of the ENSO mode is similar to the propagation of L-mode during the summer monsoon period (Murakami, 1987). However, there exists a large difference in their phase speeds, i.e., the ENSO mode is very slow, about 1/15th the phase speed of L-mode.

Wyrtki (1975) showed that oceanic Kelvin waves excited by westerly bursts over the western Pacific quickly propagate eastward across the Pacific, reaching the coast of South America within less than 3 months. In comparison, the atmospheric ENSO mode, as shown in Fig. 2, has an extremely slow phase speed approximately 1/10th or less than the oceanic Kelvin mode. Furthermore, the ENSO onset appears to occur in association with the slow eastward propagation of the ENSO mode. (The very gradual increase in u" westerlies in Fig. 1 is not due to westerly bursts, but rather is related to the propagation of the u" ENSO mode.) The ENSO mode has a very large horizontal scale (wavenumbers 1 to 2) as shown in Fig. 2, and a long time scale (more than 2 years). Therefore, it may not be possible to excite such an ENSO mode by local and temporal westerly bursts occurring over the western Pacific, as claimed by several authors (e.g., Lukas et al., 1984).

Figure 3 depicts the longitude-time section of 3-month running mean anomalies u" at the equator. The most important feature is the regular eastward propagation of both u">0 (anomalous westerly) and u"<0 (anomalous easterly) perturbations across the Indian and Pacific Oceans. An average phase speed is on the order of 0.3 m s^{-1}. Figure 3 also depicts a pronounced biennial fluctuation of the eastward propagating u" signals. Meehl (1987) and Yasunari (1988) demonstrated the biennial nature of the eastward propagating ENSO signals which involves a modulation of the annual cycle.

There exists a close association of anomalous u" westerlies (easterlies) with above (below) normal convection. This can be clearly seen in Fig. 1, which depicts a strong negative correlation between u" and OLR" over the equatorial Pacific. In Fig. 3, the amplification of anomalous westerlies (u">0) when they reach the western Pacific during the ENSO onset is significant; likewise the eastward propagation of anomalous easterlies (u"<0) during the pre-and post-ENSO phases is important. The eastward propagation of positive and negative OLR" perturbations is also clearly defined (see Fig. 5 of MS). Regions of anomalous westerlies (u">0) and above normal convection (OLR"<0) correspond to an updraft portion of the ENSO mode. This updraft portion is accompanied by anomalously high sea surface temperature (SST">0), as confirmed in MS. Conversely, regions of anomalous easterlies (u"<0) associated with below normal convection (OLR">0) and anomalous low sea surface temperature (SST"<0) represent a downdraft leg of the ENSO mode. The ENSO modes alternate between WWW (u">0, OLR"<0, SST">0) and EDC (u"<0, OLR">0, SST"<0) phases. Thus, the ENSO onset at certain fixed geographical locations is associated with changes from EDC to WWW phase, while the reverse is true during the ENSO withdrawal period. The January 1983 pattern shown in Fig. 2C is highlighted by the existence of an anomalous updraft branch over the central and eastern Pacific as contrasted with a prominent downdraft leg over the maritime continent (Sumatra, Borneo, New Guinea). Interesting, this downdraft leg (u"<0, OLR">0) appears to develop first near the western end of the Indian Ocean around July 1982 (Fig. 2B). After January 1983, the downdraft leg gradually moves eastward across the western and central Pacific. Associated with this is the alternation of updraft to downdraft over the eastern Pacific. In this vicinity, the commencement of easterly (u"<0) and dry weather (OLR">0), i.e., the ENSO withdrawal, begins around July 1983 (refer to Fig. 1C).

Yet another feature of interest in Fig. 3 is the general tendency for a weakening of u" perturbations while crossing over the maritime continent near 100°-120°E. These perturbations intensify when reaching the central and eastern Pacific. To demonstrate more clearly the changes in intensity of u" perturbations, the standard deviation of u" is computed at every 5 degrees of longitude from 50°E to 120°W along the equator during the six years of 1980-85. Computed results are shown in Fig. 4 (top), which depicts a substantially large standard deviation over the Indian Ocean, amounting to 2.1 m s^{-1} at 65°E. The standard deviation is a minimum, (0.9 m s^{-1}) at 120°E, while it reaches a maximum (2.9 m s^{-1}) near 150°W. The standard deviation for OLR" as shown in Fig. 5 (top) exhibits essentially the same features as noted in Fig. 4 (top) for u". An exact mechanism through which (u", OLR") ENSO modes change their intensity while they propagate eastward through the Indian Ocean, the maritime continent, and the Pacific Ocean is not yet known.

In order to visualize the structure of the ENSO mode, let us look at Fig. 6 which depicts the average longitudinal distribution of u", OLR", and DV" along the equator as well as the longitudinal distribution of v" along 15°N and 15°S. Here, DV" corresponds to $\partial u''/\partial x + \partial v''/\partial y$, where the second term $\partial v''/\partial y$ is estimated from v" at 15°N and 15°S. The average longitudinal distribution was computed from all composite maps over the period of January 1982 to July 1983; namely, 1 1/2 years, and with reference to the OLR" minimum which propagates very slowly eastward. Thus at the reference longitude (0°), OLR" is minimum, amounting to -45 W m^{-2} (Fig. 6). OLR" is negative all the way from -60 to +60 longitude (convective activity), while u" is westerly over the same region. This longitudinal extent (120°) defines the space scale of the ENSO mode. Equatorial westerlies reach a maximum near the reference longitude (0°) with divergence ($\partial u''/\partial x > 0$) to the west and convergence ($\partial u''/\partial x < 0$) to the east. Of particular interest is the presence of a cyclonic circulation at about -10° longitude

in each hemisphere. To the west of this twin cyclonic system are v" flows converging into the equatorial region. However, convergence due to v" is much smaller than divergence due to u", resulting in positive DV" (divergence) to the west of the reference longitude. Conversely, to the east of the reference longitude, convergence (DV"<0) with a minimum value of -1.0×10^{-6} s^{-1} occurs at +20 longitude. Why a 20^{o} longitude phase difference between DV" and OLR" perturbations exists, is not yet known. Presumably, convergence near the earth's surface rather than convergence at 850 mb could be important for the enhancement of convective activity (OLR"<0).

As mentioned earlier, Yamagata (1988) proposed an atmosphere-ocean coupled, limited region model with the initial wind and SST fields assigned for a three-month (November 1981 - January 1982) period over the western Pacific. His model successfully produced eastward moving anomalous perturbations across the central and eastern Pacific with a phase speed and an amplification rate similar to those found in Figs. 3, 4, and 5 for ENSO modes. This three-month period was characterized by anomalous u" westerlies and above normal SST" dominating the western Pacific (see Fig. 1A and Fig. 8 of MS). Thus the initial conditions Yamagata employed, primarily reflect an updraft (WWW) phase (u">0, OLR"<0, SST">0) of the ENSO mode occurring over the western Pacific. One weakness in Yamagata's model is the extraordinarily large amplification of u">0 and SST">0 perturbations near the eastern end of the Pacific as the numerical integration proceeds in time. This difficulty can be avoided by shifting the boundary conditions in the western Pacific from an updraft (WWW) to a downdraft (EDC) phase (u"<0, OLR">0, SST"<0). The assignment of an EDC phase to the western Pacific can be justified from an examination of Fig. 2C as well as Figs. 5 and 8 of MS, which all reveal the development of anomalous downdraft conditions (u"<0, OLR">0, SST">0) over the western Pacific in January 1983 when the 1982/83 ENSO reached its peak (largest amplitude of u">0, OLR"<0, SST">0) over the eastern

Pacific. Moreover these ENSO modes, as previously stated several times, have an interannual time scale and a planetary horizonal scale, and thus are distinctly different from the characteristic time and space scales of transient westerly and/or easterly bursts. The most important indication in MS is that the alternation between EDC and WWW phases over the eastern Pacific (key area for ENSO) appears to be independent of the occurrence of transient westerly and/or easterly bursts over regions far upstream. Instead the alternation is a result of the eastward propagation of ENSO modes themselves all the way from the Indian Ocean, via the maritime continent and western Pacific, to as far east as the eastern Pacific. Further study is certainly needed to identify the mechanisms through which ENSO modes develop over the Indian Ocean (birthplace).

4. Structure of intraseasonal disturbances

MS investigated the structure of intraseasonal disturbances; namely, L-, M-, and S-modes and their associated equatorial westerly bursts and convection. A composite technique was applied with reference to the (u_L, u_M, u_S) time series at the equator. Composite maps were also constructed using (OLR_L, OLR_M, OLR_S) and (v_L, v_M, v_S) time series as the reference. Comparing all of these composite patterns, it turns out that the major features are essentially identical; namely, composites are not sensitive to the difference in reference quantity, and thus they exhibit quite reliable statistical features. Consequently, subsequent discussions will be made for composite maps constructed from the (v_L, v_M, v_S) time series only. Emphasis will be placed on the nature of equatorward surges at three selected locations; i.e., the Indian Ocean (10^oS, 50^oE), the South China Sea (10^oN, 110^oE), and the western north Pacific (10^oN, 150^oE). It has been well documented that during the southern winter, strong cold surges

from the Indian Ocean penetrate into the Arabian Sea and the Indian monsoon region, occasionally facilitating the development of monsoon disturbances and associated rainfall (e.g., Krishnamurti and Bhalme, 1976). The role of strong cold surges over the South China Sea during the northern winter upon the excitation of convective active over Indonesia and northern Australia was investigated by Chang and Lau (1982). Over the western north Pacific during winter, northeasterlies of midlatitude origin frequently feed into regions of prominent equatorial westerlies and convection over the central Pacific (Sumathipala and Murakami, 1988).

For L-mode, separate composites are made for northern summer (May-October; MJJASO) and winter (November-April; NDJFMA), hence facilitating the investigation of differences in characteristic features between the two seasons. Composite maps with reference to v_L over the Indian Ocean in MJJASO are constructed as follows: Using the time series of daily v_L at 10^oS, 50^oE as shown in Fig. 7, we select the first sampling date when v_L is largest (southerly) during the six northern summers of 1980-85; next we select the second largest value, and we continue this process until we have the 10th maximum value, all exceeding 1 m s^{-1}. In Fig. 7, open circles indicate the selected 10 sampling dates for MJJASO. We then computed the 10-day average u_L, v_L, and OLR_L not only at the reference point (10^oS, 50^oE), but over a larger surrounding region. However 10-day mean values far away from the reference point are not reliable; therefore we restrict our compositing to an area covering a 40^o latitude span (20^oS-20^oN) and 160^o longitude span (0^o-160^oE). For brevity, these mean maps are signified as "$v_L(+)$" composites. Similarly we construct $v_L(-)$ composite maps, utilizing the first ten sampling days for unusually small (northerly) v_L values at the reference point (refer to black dots in Fig. 7). Composite maps for the $v_L(-)$ case are nearly identical, except for a change of sign, to those for $v_L(+)$ case. The local statistical significance of the

difference between the two composite cases is tested by the procedure described by Panofsky and Brier (1958). For brevity, the areal percentage that surpasses the local 95% confidence level is signified as "LS." In order for a composite map to be spatially significant, LS should exceed a certain critical value (Livezey and Chen, 1983). This critical value for area significance is determined from a Monte Carlo experiment (refer to Murakami, 1987), and is signified as "AS." A composite map is considered to be significant if LS for this particular composite is greater than AS. The composite map thus computed for MJJASO is shown in Fig. 8A. Similarly, the compositing technique is also applied when constructing the map for NDJFMA, which is depicted in Fig. 8B.

In Fig. 8A for MJJASO, LS for the streamfunction ψ_L is 39%, which exceeds the corresponding AS value of 37%. Therefore ψ_L surpasses the 95% statistical confidence level. By definition, v_L is a maximum (1.3 m s^{-1}) at 10°S, 50°E. Equatorward v_L cold surges (heavy arrow in Fig. 8A) from the Southern Hemisphere midlatitudes converge into a region of equatorial westerlies and convection (thin full lines) over the eastern Indian Ocean. Equatorial westerlies exist between a pair of tropical cyclonic disturbances which are nearly symmetric with respect to the equator — one to the north, and one to the south. The longitudinal extent of these equatorial westerlies is large, amounting to about 60° (50°-110°E); this however, is still much smaller than the horizontal scale of the ENSO mode which is approximately 120° as shown in Fig. 6. The equatorial westerlies reach a maximum (2.5 m s^{-1}) around 85°E, that is, about 35° downstream of the reference longitude (50°E).

Yet another feature of interest in Fig. 8A is the existence of an anomalous east-west extended trough (see dashed line in Fig. 8A) along about 10°-15°N over the Arabian Sea. South of this E-W trough are anomalous westerlies and active convection (OLR_L<0). This is contrasted with easterly anomalies and below normal

convection (OLR_L>0) to the north of the E-W extended trough. Thus, summer monsoons over central India and Indochina are less active than normal (break monsoons), when cold southerly surges are strongest over the Indian Ocean at the sampling dates (open circles in Fig. 7). South Asian summer monsoons alternate between break and active phases in association with the northward progression of anomalous E-W extended troughs on 30-60 day time scales. This can be confirmed by constructing composite maps using different (time lag) sampling dates (not shown). In summary, L-mode plays an important role in the intraseasonal variations of the South Asian summer monsoon, as previously pointed out by Krishnamurti and Subrahmanyam (1982), and Murakami and Nakazawa (1985).

The composite map for the Indian Ocean NDJFMA case (Fig. 8b) barely passes the 95% areal confidence level. Equatorial u_L westerlies over the Indian Ocean are less organized and much weaker than in MJJASO. To the east of the reference point (10°S, 50°E) is centered a cyclonic cell with relatively strong southerlies prevailing off the east coast of South Africa. This cyclonic cell, which surpasses the local 95% confidence level (light mesh in Fig. 8A), perhaps reflects disturbance activity in and around the intertropical convergence zone in NDJFMA.

Our study also includes composite maps for M-modes during four seasons, i.e., JJA (Jun.-Aug.), SON (Sept.-Nov.), DJF (Dec.-Feb.), and MAM (Mar.-May). In each three-month period, we selected 10 sampling dates utilizing the time series of daily v_M (Fig. 7), in exactly the same manner as we determined the 10 sampling dates for the L-mode using the v_L time series. Composites of M-mode with reference to v_M at (10°S, 50°E) for all four seasons are shown in Figs. 9A-D. The most noteworthy feature is the asymmetry with respect to the equator. Characteristically, the horizontal extent of disturbances is not as large as that for L-mode (Fig. 8), therefore M-mode plots are limited to 120° of longitude. In JJA strong southerly surges to the west of a

Southern Hemisphere trough penetrate into the Indian monsoon region. Equatorial westerlies and convective activity are weak to moderate, and are confined to a small area between about 50^{o} and 70^{o}E. This stands in sharp contrast with a large area of prominent equatorial convection and westerlies (bursts) for the L-mode (Fig. 8A). The composite map for the M-mode in SON (Fig. 9B) just passes the 95% significance level, and exhibits a similar pattern as in JJA, that is, a trough in the Southern Hemisphere with southerly surges to the west and minimal equatorial convection. The DJF and MAM patterns, on the other hand, show a different character with a cyclonic cell east of Madagascar and a relatively long stretch ($>30^{o}$) of equatorial westerlies.

For S-mode (Fig. 10), the composite maps for JJA, SON, and MAM are all statistically insignificant (LS<AS). This is due to substantial fluctuations of (u_S, v_S, OLR_S) values from one day to the next within the selected 10 days for compositing. A couple of features, even though based on tenuous statistical significance, are worth pointing out: (1) The longitudinal extent of u_S along the equator is only 20^{o} or less, and (2) v_S is as strong as u_S, indicating the importance of meridional winds as compared with zonal winds for S-mode. In comparison, L-mode is characterized by the predominance of zonal winds as the equator is approached (refer to Fig. 8).

The South China Sea is known for strong low-level northerly surges emanating from Siberia in the northern winter, occasionally exceeding 10 m s^{-1} [see Fig. 11 (top)]. The composite maps constructed with reference to v_L at 10^{o}N, 110^{o}E are shown in Fig. 12. Since the MJJASO composite pattern does not satisfy the 95% confidence level, our discussion will be limited for the most part to NDJFMA composite, which shows little influence of v_L surges over the South China Sea upon the induction of equatorial westerlies (u_L) and convection (OLR_L). This is in qualitative agreement with the findings by Sumathipala and Murakami (1988). However, we see some indication of convective activity (anomaly)

extending southeastward from Borneo, through New Guinea, to the South Pacific convergence zone (SPCZ). Hence, v_L surges over the South China Sea may have exerted some measures of control upon the Southern Hemisphere monsoon activity. Also note in Fig. 12B that weak equatorial easterlies are present over the Indian Ocean. In comparison, Fig. 12A for MJJASO exhibits more prominent equatorial easterlies over the Indian Ocean. These easterlies are sandwiched between a pair of anticyclonic cells which are nearly symmetric with respect to the equator.

The composite patterns constructed with northerly v_M over the South China Sea as reference are shown in Fig. 13. One immediately notes a strong seasonality. In DJF cold northeasterly surges do not induce significant westerlies along the equator; however, these strong surges do lead to cross-equatorial flows between Sumatra and Borneo, and to the enhancement of monsoonal westerlies ($u_M>0$) and monsoon rains ($OLR_M<0$) near Indonesia. In MAM northerly v_M surges over the South China Sea turn anticyclonically into the Bay of Bengal as anomalous easterlies ($u_M<0$). As in DJF, no significant westerlies are induced along the equator. In JJA a distinct cyclonic cell near the Philippines probably indicates the tropical disturbance activity in northern summer. In contrast, the Southern Hemisphere circulation is generally weak with no major disturbance activity. Thus, the (u_M, v_M) circulation in JJA as shown in Fig. 13A is asymmetric with respect to the equator and no westerlies are present along the equator. Circulation features in SON are similar to those in JJA.

Of special interest in the composite maps for S-modes (Fig. 14) is the presence of substantially strong cross-equatorial northerlies between Sumatra and Borneo in all four seasons. In particular, cross-equatorial northerlies are strongest in SON and DJF, and are probably responsible for increased rains ($OLR_S<0$) over the Indonesian region. This indicates the development of anomalous local Hadley circulations on 1 to 6 day time scales along about $110^{\circ}E$ during SON and DJF. Over the Indian Ocean, on

the other hand, cross-equatorial v_S flows, which represent the low-level branch of anomalous (1-6 day) local Hadley circulation, are much less organized, as was already shown in Fig. 10.

The time series of daily meridional winds over the western Pacific (10^oN, 150^oE) is shown in Fig. 15. It reveals the occurrence of exceptionally strong southerlies during the 1982 summer and fall (initial stage of the 1982/83 ENSO). Most probably, this reflects an unusual development of tropical depressions over the western Pacific, as indicated by large amplitudes of v_S and v_M fluctuations during the same period. In comparison, 30-60 day v_L fluctuations are much less pronounced.

By utilizing the time series of v_L at 10^oN, 150^oE (Fig. 15), composites were made for both the $v_L(+)$ case (open circles) and the $v_L(-)$ case (black dots). Since the two composites exhibit identical features (without regard to sign), Fig. 16 presents the composite patterns for the $v_L(-)$ case only. In NDJFMA (Fig. 16B), moderate v_L surges split: one branch flows to the central Pacific where equatorial westerlies sandwiched between 2 cyclonic cells are enhanced (about 2 m s^{-1}), and the other branch feeding into the western Pacific and the maritime continent where weak equatorial easterlies (about 1 m s^{-1}) are accompanied by below normal convection ($OLR_L>0$). Namely, we see the development of an anomalous (30-60 day) Walker circulation with updraft portion ($u_L>0$, $OLR_L<0$) to the east and downdraft portion ($u_L<0$, $OLR_L>0$) to the west of the reference longitude 150^oE. The longitudinal extent of equatorial westerlies is 80^o or longer. In short, the western Pacific appears to be most favorable for the excitation of equatorial westerlies due to cold surges from the winter hemisphere midlatitudes, while wintertime cold surges over the South China Sea do not enhance equatorial westerlies on 30-60 day time scales (Fig. 12B).

Keen (1982) found that transient westerly bursts at the equator become very strong when twin tropical cyclones develop on each side of the equator. Our contention is that such twin

tropical cyclones tend to develop more frequently over the western Pacific during the westerly phase ($u_L>0$) of L-mode (30-60 day oscillation). The reason is as follows: In Fig. 16B, L-mode over the western Pacific near 180° has a distinct symmetric character with respect to the equator, and thus resembles the equatorial Kelvin wave. As will be discussed later, neither M-mode nor S-mode is symmetric with reference to the equator, therefore conditions are unfavorable for the development of twin tropical cyclones over the western Pacific.

The composite maps for M-mode (Fig. 17) display a strong seasonality with an asymmetric character with respect to the equator. In DJF it is of particular interest that a prominent trough dominates the winter hemisphere (western Pacific), exemplifying a possible midlatitude-tropical interaction on 7-20 day time scales. Thus, M-mode is not an equatorially trapped mode. The DJF composite also depicts the following features: (1) To the west of the winter hemisphere trough are northerly v_M flows which penetrate deep into the Southern Hemisphere monsoon region after crossing the equator east of New Guinea, and (2) u_M is positive (westerly) and substantial (about 1 m s^{-1}) near 160°E at the equator. On the other hand, the JJA and SON composite patterns show the presence of an anticyclonic cell centered near 15°N, 140°E. To the east of this anticyclone are prominent northerly v_M flows. Recall that the $v_M(+)$ composites display reverse features with a prominent cyclonic cell at 15°N, 140°E and strong southerlies dominating to its east. This is largely associated with unusually strong disturbance activity during the early stage of ENSO (1982 summer and fall), as seen earlier in Fig. 15 (top).

Now let us look at the characteristics of S-mode. The $v_S(-)$ composite in DJF (Fig. 18C) depicts a narrow zone of northerly surges extending toward the equator. The MAM composite reveals similar features. These northerly surges neither generate equatorial westerlies (which may serve as the energy source for

oceanic Kelvin waves) nor enhance equatorial convection, rather they cross the equator and increase convection in a limited region of the Southern Hemisphere. These characteristics are closely shared by the northerly v_S surges in the South China Sea (Fig. 14). At any rate, the S-mode is characterized by the dominance of the meridional over the zonal component of the winds.

The ratio between the zonal and meridional components of wind is an important indicator of the nature of the disturbances in question. We express the magnitude of the zonal wind component as $|u|$, and of the meridional component as $|v|$. The ratio $|v|/|u|$ differs significantly with the period of disturbances. For example, for steady equatorial waves as treated by Gill (1980), the ratio between $|v|$ and $|u|$ is extremely small, on the other hand for midlatitude disturbances which are of the Rossby-wave type, $|v|$ is as important as $|u|$; namely, the ratio is nearly one. Figure 19A shows latitudinal distribution of $\overline{|u_L|}$, $\overline{|v_L|}$, and $\overline{|v_L|}/\overline{|u_L|}$. Here, $\overline{|u_L|}$ and $\overline{|v_L|}$ signify the zonal mean value of $|u_L|$ and $|v_L|$ averaged between 50^oE and 120^oW throughout the entire 6 years (1980-85). In the equatorial channel between 5^oN and 10^oS, $\overline{|u_L|}$ is large while $\overline{|v_L|}$ is small. In particular, $\overline{|u_L|}$ is maximum (0.6 ms^{-1}) at the equator and $\overline{|v_L|}/\overline{|u_L|}$ is a minimum (0.3). This implies that L-mode exhibits characteristics similar to Kelvin waves. Next we examine Fig. 19B, where the following features are noted: (1) $\overline{|u_M|}$ is relatively uniform with respect to latitude, amounting to 0.4 ms^{-1}, (2) at all latitudes $\overline{|v_M|}$ is greater than $\overline{|v_L|}$, and (3) $\overline{|v_M|}/\overline{|u_M|}$ amounts to 0.5 in the extratropical latitudes, while it is only about 0.25 in the equatorial channel. As such, M-mode in the equatorial region with a nearly constant small ratio $\overline{|v_M|}/\overline{|u_M|}$ is similar, in some degree, to L-mode which has the smallest ratio $\overline{|v_L|}/\overline{|u_L|}$ at the equator. S-mode has a different character with $\overline{|v_S|}/\overline{|u_S|}$ amounting to about 1.0 throughout all the latitudes.

5. Zonal phase propagation of equatorial u_L, u_M, and u_S perturbations

The previous section emphasized the differences in space characteristics of equatorial intraseasonal disturbances with respect to their periodicity. This section will highlight the differences in time characteristics among equatorial L-, M-, and S-modes. It can be expected that the direction and speed of phase propagation may be quite different from one mode to another. In addition, each mode may change its intensity (amplitude) while propagating zonally along the equator. Together Sections 4 and 5 provide necessary and sufficient information for further testing, either qualitatively or quantitatively, of the westerly burst concept.

The existence of 30-60 day oscillations in the tropics has been confirmed by many authors; e.g., Madden and Julian (1972), Yasunari (1980), Krishnamurti and Subrahmanyam (1982), Murakami and Nakazawa (1985), and Lau and Chan (1985). All of these studies identified planetary-scale, eastward propagating (8° long. day^{-1}) 30-60 day perturbations across the equatorial Indian and Pacific Oceans.

A variety of zonally propagating waves in the trade wind regime has been documented, based mainly on spectrum analysis of conventional radiosonde data (Yanai et al., 1968; Wallace and Chang, 1969; Chang et al., 1970; Murakami and Ho, 1972). These spectral studies reveal the presence of spectral peaks near 5°-15° latitude in the period range of 3-5 days, 7-10 days, and 16-25 days. However, considerable discrepancies exist among the various studies concerning detailed interpretation of the results. The wavelength (~4000 km) and phase speed (~10 m s^{-1}) of the first type of disturbance with a period of about 4 days agrees well with those of classical easterly waves, as determined by Reed and Recker (1971). Recently, Murakami et al. (1986) noted that along 15°N over the Asiatic monsoon region (40°-160°E), the 30-60 day

perturbations move eastward, while transient disturbances with periods shorter than 30 days move westward. On the other hand, based on 3-hourly Japanese Meteorological Satellite infrared data, Nakazawa (1988) showed that an ensemble of cloud clusters (signified as "super cluster") tends to propagate eastward with a speed of about 10-15 m s^{-1}, while individual cloud clusters within a super cluster move westward along the equator. These studies cited above clearly demonstrate the differences in phase propagation (direction and speed) with respect to the time and space scales of equatorial transient disturbances. The remainder of this section focuses on the zonal phase propagation of L-, M-, and S-modes along the equator.

Figures 20 and 21 depict longitude-time sections of OLR_L and u_L, respectively, between 50°E and 120°W along the equator. One can see many occasions of systematic eastward propagation of equatorial L-modes across the Indian Ocean and the western Pacific. This is best exemplified by the eastward propagation of westerly u_L perturbations (Fig. 21) during the following periods: 20 November 1981 - 2 January 1982 (denoted as L1); 11 March - 13 April 1982 (L2); 18 April - 12 May 1982 (L3); 28 May -22 July 1982 (L4); 6 July - 21 July 1982 (L5); and 8 August - 22 September 1982 (L6). An average eastward phase speed for these westerly u_L perturbations is about 5 to 6 m s^{-1}. In general, the eastward propagation is more clearly defined in the 30-60 day zonal wind perturbations at 200 mb than at 850 mb (Murakami and Nakazawa, 1985). Lau and Chan (1985) claimed the intensification of L-mode prior to the 1982/83 ENSO onset. However, a comparison between Fig. 3 for u" and Fig. 21 for u_L indicates that the occurrence of u_L westerly bursts is independent of the ENSO onset over the central and eastern Pacific. In fact, strong u_L westerly bursts in excess of 3 m s^{-1} are seen as early as 10 December 1981 in association with the eastward passage of L1 near 140°E. Further examination of Fig. 21 reveals, that between about March and July 1982 during the easterly phase of u" over the Indian Ocean, an

increase in the frequency of strong westerly u_L perturbations occurs in the same vicinity. Perhaps, the point to be made here is that u_L westerly bursts are occurring all the time over the Indian Ocean, but they tend to intensify during the pre-ENSO phase of March to July 1982. Also of interest is the tendency for u_L (or OLR_L) perturbations to dissipate before reaching the central Pacific prior to ENSO, while they tend to travel as far eastward as the eastern Pacific after the ENSO onset. This is associated with changes in u" from easterly prior to ENSO to westerly during the mature phase of ENSO over the eastern Pacific (Fig. 3). Here, our contention is that individual L-modes do not appear to contribute much to the ENSO onset over the central and eastern Pacific (key area for ENSO).

Typical westward propagation of u_M perturbations is exemplified by M1, M2, and M3 in Fig. 22, showing the longitude-time section of u_M at the equator. These u_M westerly perturbations have an average phase speed of about 9 m s^{-1} (easterly). Normally, the westward phase propagation can be seen more clearly over the Pacific Ocean than over the Indian Ocean. Occasionally, however, u_M disturbances can be traced all the way from the eastern Pacific to the western Indian Ocean. For example, M3 has a long life span of more than one month from 120°W on 14 November 1982 to 50°E around 21 December 1982. Thus, u_M westerly bursts can occur all along the extensive trajectory of the M3 perturbation.

Let us next turn our attention to Fig. 23 for S-mode. One at once notes that the phase propagation is not as well defined as in M-mode. The general tendency for westward propagation is frequently interrupted by either stagnation or eastward propagation. In Fig. 23, seven u_S disturbances (labeled S1 to S7) exhibit regular westward phase propagation with an average speed of about 15 m s^{-1}.

In Figs. 21 to 23, substantial changes in intensity (amplitude) of u_L, u_M, and u_S perturbations as they propagate

zonally (either eastward or westward) are apparent. For example, Fig. 21 shows that eastward propagating u_L perturbations weaken considerably while crossing over the maritime continent (100°-130°E). Similarly, the maritime continent is characterized by minimum amplitude for the westward moving u_M and u_S perturbations (Figs. 22 and 23). To demonstrate this more clearly, the standard deviation of u_L, u_M, and u_S is computed at every 5 degrees of longitude along the equator during the six years of 1980-85. Computed results are shown in Fig. 4. As expected, the standard deviations for all intraseasonal u_L, u_M, and u_S perturbations are minimum over the maritime continent. In contrast, the standard deviations attain their maximum value over the Indian Ocean (85°E) and the western Pacific (140°E). These are two of the most favorable regions for the occurrence of strong u_L, u_M, and u_S westerly (or easterly) bursts. The standard deviations for OLR_L, OLR_M, and OLR_S as shown in Fig. 5 are also largest over the central Indian Ocean and the western Pacific. At present, it is not yet known exactly why the activity of intraseasonal disturbances is most pronounced over these two oceanic regions. Why is the intraseasonal disturbance activity not uniformly distributed throughout the tropics? The implication is that it is not of a purely zonal propagating character. It is then highly probable that the nature of intraseasonal L-, M-, S-modes could be quite different and exhibit regional characters.

The minimum intraseasonal disturbance activity over the maritime continent is also worth paying attention to. This is a region of smallest amplitude for the interannual u" and OLR" perturbations as shown in Figs. 4 and 5 (top). By applying harmonic analysis to OLR data, Murakami et al. (1986) found that the amplitude of the first two harmonics, which represents the yearly and half-yearly cycles, respectively, is the smallest in the Sumatra-Borneo-New Guinea region. Namely, this is a region of minimal monsoon activity. On the other hand, Houze et al. (1981) reported that diurnal variations in convection are far more

pronounced over the maritime continent than any other tropical region. Thus diurnal variations play an important role in releasing a large amount of latent heat through convection. Perhaps, they are more important than intraseasonal L-, M-, and S-disturbances in the production of atmospheric heat sources over and around the maritime continent.

No daily SST data has been available in the present study. This inhibits the investigation into intraseasonal variations of SST. With respect to the 30-60 day period band, Murakami (1988b) found a distinct negative correlation between SST_L and OLR_L over the equatorial Arabian Sea and the Bay of Bengal, where the SST data coverage is sufficient to determine daily SST values. The largest negative correlation occurs at the 10 to 15 day lag (SST_L leading). This means that convection becomes most active ($OLR_L<0$) about 10-15 days after the occurrence of highest SST_L anomaly. Since OLR_L is inversely correlated with u_L, the strongest westerly u_L anomaly tends also to occur about 10-15 days after anomalously warm SST_L. (The amplitude of SST_L is on the order of $0.5^{o}C$.) Thus, the interactive nature of the ocean appears to be quite important in the development of atmospheric 30-60 day oscillations. Observational information is scanty pertaining to SST_M (7-20 day) and SST_S (1-6 day) variations. Because of the short periodicity involved, both SST_M and SST_S are expected to be much smaller in magnitude than SST_L. Our speculation is that u_M and u_S westerly (or easterly) bursts could not produce any significant oceanic response in sea surface temperature. Further study is needed to confirm this speculation.

6. Interannual changes in the activity of u_L, u_M, and u_S perturbations

Because of the difference in time and space scales, no correlation exists between intraseasonal (u_L, u_M, u_S) modes and

the interannual u" mode. Nevertheless, there has to be some relationship between the two modes, therefore we next computed kinetic energy K_L, K_M, and K_S every day during the six years of 1980-85. The normal annual cycle was determined from K_L, K_M, and K_S values for each day of the year over all years (1980-85). This normal annual cycle was then removed from the 3-month running mean K_L, K_M, K_S values. Interannual components, which are denoted as K_L'', K_M'', K_S'', indicate the change in activity of u_L, u_M, and u_S zonal wind bursts (either westerly or easterly) on the interannual time scale. Here, the central problem is to examine the relationship between interannual u" modes and the year-to-year variations in (K_L'', K_M'', K_S'') activity.

Figure 24 indicates the evolution of K_L'' (thin full lines), as well as the eastward progression of westerly u" perturbations (heavy full line) across the Indian and Pacific Oceans. Over the central Indian Ocean around 80°E, we see no significant correlation between K_L'' and u". In this vicinity, extraordinarily strong K_L'' activity between March and July 1982 coincides with near zero or slightly negative (easterly) u", while between July and September 1981 moderate K_L'' activity is associated with distinct westerly u" anomalies (refer to Fig. 3). Conditions are different over the western Pacific (140°E), where K_L'' is substantially large (0.5-1.0 m^2s^{-2}) during the pre-ENSO phase from July to December 1981, and later reaches a maximum (1.3 m^2s^{-2}) at the same time as u" westerlies become strongest around March-April 1982 (ENSO peak phase over the western Pacific). This is followed by the drastic reduction in K_L'' activity after about the 1982 summer. Further east between about 160°E and 180°, K_L'' becomes most pronounced about 1 to 3 months after the occurrence of maximum u" westerlies. East of the date line over the eastern Pacific, K_L'' is small, and hence 30-60 day perturbations contribute little to the in situ development of interannual ENSO modes. In short, over the western Pacific between 140°E and 180°, there exists a direct relationship between frequency of occurrence and the amplitude of the 30-60 day

u_L oscillation and u" anomaly fields. In this vicinity, groups of u_L westerly (or easterly) events, as expressed by K''_L, appear to have some association with interannual u" fluctuations over the same region. There is no indication of K''_L over the Indian Ocean as well as the western Pacific acting as a remote forcing for the enhancement of u" perturbations further downstream (the eastern Pacific).

The longitude-time section of K''_M shown in Fig. 25 provides useful information pertaining to a possible nonlinear interaction between interannual u" perturbations and u_M transients. Lukas et al. (1984) claimed the occurrence of strong transient westerly bursts over the western Pacific prior to an ENSO onset. Between about 130°E and 180° in Fig. 25, K''_M is certainly above normal in the second half of 1981, thus implying the development of groups (ensemble) of strong u_M bursts during the pre-ENSO phase. However, whether this really supports the westerly burst concept is questionable. Here, our contention is as follows:

(1) The occurrence of large K''_M over the western Pacific during the period from July 1981 to about March 1982 precedes the arrival of interannual westerly u" modes to the eastern equatorial Pacific by more than one year. In Fig. 25, note that u" westerlies reach the longitude 120°W around April 1983. This one year or slightly longer period is approximately four times as large as the time requirement for oceanic Kelvin waves to travel through the entire Pacific from the western to eastern end.

(2) In Fig. 25, a distinct zone of large K''_M tends to propagate eastward from about 180° on September 1982 to 120°W in April 1983; hence, its phase speed is very slow and nearly identical to that of the westerly u" mode. Even though individual u_M disturbances generally move westward (Fig. 22), groups of u_M events; i.e., K''_M, propagate very slowly eastward (0.3 m s^{-1}). At any rate, Fig. 25 provides evidence that over the eastern Pacific between 180° and 120°W, K''_M activity becomes above normal, nearly following the trajectory of maximum u" westerlies; although above normal K''_M

activity tends to lead u" westerlies by about 3 to 5 months. Namely, a group of space-overlapping and time-clustering u_M intraseasonal disturbances over the eastern Pacific probably provides the energy for the in situ enhancement (or maintenance) of interannual u" westerlies there. Our speculation is that remote forcing, attributed to u_M bursts over the western Pacific, contributes little to the enhancement of u" modes over the eastern Pacific.

To further substantiate interannual variations of the intraseasonal disturbance activity, correlations were computed for K_L'', K_M'', and K_S'' using u" as the reference time series at every 5 degrees of longitude along the equator from 50°E to 120°W during the six years of 1980-85. A correlation coefficient greater than 0.41 is significant at the 95% confidence level. The simultaneous (no lag) correlation between u" and K_L'' (Fig. 26C) exceeds the 95% confidence level over the western Pacific between about 140°E and the date line, while it is quite small, although positive, over the eastern Pacific where the activity of 30-60 day oscillations is generally weak. In Fig. 26B, simultaneous correlation between u" and K_M'' is positive everywhere along the equator from 50°E to 120°W. Of particular interest is a marked band of large correlation in excess of +0.45 from the date line at lag -10 months to 120°W at lag -1 to -2 months (K_M'' leading). This means that the eastern Pacific (180°-120°W) is characterized by strong activity of u_M modes prior to and during the WWW phase of interannual ENSO modes, perhaps indicating an in situ nonlinear coupling between the two modes over that region, as speculated earlier. The correlation between u" and K_S'' is positive over the central and eastern Pacific (Fig. 26A). Thus, u_S transients are also responsible for the enhancement and maintenance of interannual u" modes over the same region.

7. Concluding remarks

Data utilized in this study are ECMWF 850 mb winds, and outgoing longwave radiation (OLR) during the six years of 1980-85. The highlight of this period is the occurrence of the 1982/83 ENSO. Some of the characteristic features of ENSO modes are described in terms of three-month running mean anomalies, which are signified as u", v", and OLR", respectively. Daily OLR and 850 mb winds are subjected to a band-pass filter to obtain climatological information on equatorward surges, equatorial westerly bursts and convection. These filtered data are denoted as u_L, v_L, and OLR_L (30-60 day); u_M, v_M, and OLR_M (7-20 day); and u_S, v_S, and OLR_S (1-6 day), respectively. For brevity, (u_L, v_L, OLR_L) is termed L-mode, (u_M, v_M, OLR_M) denotes M-mode, and (u_S, v_S, OLR_S) is defined as S-mode. These intraseasonal L-, M-, and S-modes are clearly separate from interannual ENSO (u", v", OLR") modes.

Section 3 described the nature of ENSO modes. The eastward propagation of positive u" (westerly) and negative OLR" (above normal convection) perturbations across the Indian and Pacific Oceans is well defined; likewise, the eastward progression of negative u" (easterly) and positive OLR" (below normal convection) anomalies is significant. At any fixed geographical location (for example, the eastern Pacific), the alternation between the easterly and dry ($u"<0$, $OLR">0$) phase and the westerly and wet ($u">0$, $OLR"<0$) phase is a result of the eastward propagation of ENSO modes themselves. Transient westerly and/or easterly bursts occurring over regions far upstream seem to contribute little to phase changes of ENSO episodes. The eastward phase speed of ENSO modes is approximately 0.3 m s^{-1}, being one order of magnitude smaller than the corresponding phase speed of oceanic Kelvin waves. The birthplace of ENSO modes appears to be the western end of the Indian Ocean. These modes weaken considerably while passing through the maritime continent (Sumatra, Borneo, New

Guinea), followed by an anomalous amplification when they reach the central Pacific.

Section 4 detailed the differences and similarities in the horizontal structural features of intraseasonal L-, M-, and S-modes with different locations and periodicities. The main results are summarized as follows:

L-mode

The western Pacific during northern winter and the Indian Ocean during southern winter display strong equatorial westerlies ($u_L>0$) and convection ($OLR_L<0$) which are associated with equatorward cold surges from the winter hemisphere midlatitudes. In comparison, wintertime cold v_L surges over the South China Sea do not enhance equatorial westerlies and convection on 30-60 day time scales. Over the central Indian Ocean and the Pacific, L-mode exhibits a symmetric character with equatorial westerlies sandwiched between two cyclonic cells, one to the north, and one to the south of the equator. The longitudinal extent of equatorial westerlies is large amounting to about 80^{o} (Figs. 8A and 16B); this however, is still much smaller than the scale of the ENSO mode which is approximately 120^{o} (Fig. 6).

M-mode

The most noteworthy features are a strong seasonality and an asymmetric character with respect to the equator. Thus M-mode is not an equatorially trapped mode. Characteristically, the longitudinal extent of westerlies along the equator (which may serve as the energy source for oceanic Kelvin waves) is small, confined to only about 30^{o}. Over the South China Sea during the northern winter, cold northerly v_M surges are very strong, but do not induce significant westerlies along the equator; however, these strong surges do lead to cross-equatorial flows near Singapore, and to the enhancement of monsoonal westerlies and rains over the Indonesian-northern Australian region.

Similarly, southerly v_M surges off the east coast of Africa during the southern winter, although weak, penetrate into the Indian monsoon region, implying a possible midlatitude-tropical interaction on 7-20 day time scales.

S-mode

The S-mode is characterized by the dominance of the meridional over the zonal component of the winds, while the L-mode is primarily associated with zonal winds as the equator is approached. Over the South China Sea and the western north Pacific during the northern winter, a narrow zone of strong northerly surges extends toward the equator. These northerly surges neither generate equatorial westerlies nor enhance equatorial convection. These v_S surges represent the low-level branch of a local Hadley circulation on 1 to 6 day time scales. Over the Indian Ocean, v_S surges are less organized and statistically insignificant.

Section 5 highlighted the differences in zonal phase propagation among L-, M-, and S-modes. L-modes exhibit a systematic eastward phase propagation (5 to 6 m s^{-1}) across the equatorial Indian Ocean and the western Pacific. The enhancement of individual u_L westerly (easterly) bursts over the western Pacific appears to be independent of the ENSO onset (withdrawal) over the eastern Pacific. M-modes generally propagate westward with an average phase speed of 9 m s^{-1}. Occasionally, u_M disturbances can be traced all the way from the eastern Pacific to the western Indian Ocean. On these occasions, u_M westerly (or easterly) bursts can occur all along their extensive trajectory. The phase propagation of S-modes is not as well defined as L- and M-modes. The general tendency for u_S to propagate westward is frequently interrupted by either stagnation or eastward propagation. The Indian Ocean (85°E) and the western Pacific (140°E) are two of the most favorable regions for the occurrence of strong u_L, u_M, and u_S westerly (or easterly) bursts. On the other hand, the maritime continent is characterized by minimum

amplitudes of u_L, u_M, and u_S perturbations; namely, they weaken near the Sumatra-Borneo-New Guinea region.

Section 6 discussed the relationship between interannual u" modes and 3-month running mean anomaly eddy kinetic energy (K''_L, K''_M, and K''_S), which represents an ensemble effect of u_L, u_M, and u_S bursts. The simultaneous (no lag) correlation between u" and K''_L exceeds the 95% confidence level over the western Pacific between about 140°E and the date line. Further east over the eastern Pacific, no significant correlation exists between u" and K''_L, indicating that 30-60 day perturbations contribute little to the in situ development of interannual ENSO modes. The lag correlation between u" and K''_M is large and significant over the eastern Pacific. Of particular interest is a large positive correlation in excess of +0.45 between 180° and 120°W at lag -10 to -2 months (K''_M leading), perhaps indicating an in situ nonlinear coupling between interannual u" modes and intraseasonal M-modes over the eastern Pacific. S-modes are also responsible for the maintenance of u" perturbations over the same region.

One of the most important future research problems concerns the mutual relationship among atmospheric ENSO modes, intraseasonal (L, M, S) modes, and oceanic SST variations. The main objective is to explain why ENSO modes and all intraseasonal components weaken considerably near the maritime continent (Sumatra, Borneo, New Guinea) and the Indonesian Seas where the long-term average SST is quite high. Furthermore, the interactive role of the ocean in the development of atmospheric variations on interannual as well as intraseasonal time scales requires additional investigation.

Acknowledgments

The authors are indebted to Mrs. Dixie Zee for her assistance in data processing and final editing of this manuscript.

This research has been supported by the National Science Foundation under Grant ATM 86-09968.

APPENDIX

List of Acronyms and Symbols

OLR	outgoing longwave radiation
SST	sea surface temperature
ENSO	El Nino/Southern Oscillation
ECMWF	European Centre for Medium Range Forecasts
( )"	3-month running mean anomaly data
ENSO mode	(u", v", OLR") fields
WWW phase	u" > 0, OLR" < 0, SST" > 0
EDC phase	u" < 0, OLR" > 0, SST" < 0
$( )_S$	2-6 day filtered data
$( )_M$	7-20 day filtered data
$( )_L$	30-60 day filtered data
S mode	(u_S, v_S, OLR_S) fields
M mode	(u_M, v_M, OLR_M) fields
L mode	(u_L, v_L, OLR_L) fields
MJJASO	May-Jun-Jul-Aug-Sep-Oct
NDJFMA	Nov-Dec-Jan-Feb-Mar-Apr
JJA	Jun-Jul-Aug
SON	Sep-Oct-Nov
DJF	Dec-Jan-Feb
MAM	Mar-Apr-May
K_S	$u_S^2/2$
K_M	$u_M^2/2$
K_L	$u_L^2/2$
K_S"	3-month running mean anomaly K_S

K_M''	3-month running mean anomaly K_M
K_L''	3-month running mean anomaly K_L
$\overline{(\ )}$	zonal mean or monthly mean
$\lvert\ \rvert$	absolute value
$\langle\ \rangle$	3-month running mean

References

Barnett, T.P., 1977: An attempt to verify some theories of El Nino. J. Phys. Oceanogr., 7, 633-647.

_____, 1981: Statistical relations between ocean/atmospheric fluctuation in the tropical Pacific. J. Phys. Oceanogr., 11, 1043-1058.

_____, 1983: Interaction of the monsoon and Pacific trade wind system at interannual time scales. Part I: The equatorial band. Mon. Wea. Rev., 111, 756-773.

Busalacchi, A.J., and J.J. O'Brien, 1981: Interannual variability of the equatorial Pacific in the 1960s. J. Geophys. Res., 86, 10901-10907.

Chang, C.P., V.F. Morris and J.M. Wallace, 1970: A statistical study of easterly waves in the western Pacific: July-December 1964. J. Atmos. Sci., 27, 195-201.

_____, and K.-M. Lau, 1982: Short-term planetary-scale interactions over the tropics and midlatitudes during northern winter. Part I: Contrasts between active and inactive periods. Mon. Wea. Rev., 110, 933-946.

Eriksen, C., M. Blumenthal, S. Hayes and P. Ripa, 1983: Wind-generated equatorial Kelvin waves observed across the Pacific Ocean. J. Phys. Oceanogr., 13, 1622-1640.

Gill, A.E., 1980: Some simple solutions for heat-induced tropical circulations. Quart. J. Roy. Meteor. Soc., 106, 447-462.

Harrison, D.E., 1987: Monthly mean island surface winds in the central tropical Pacific and El Nino events. Mon. Wea. Rev., 115, 3133-3145.

_____, and P.S. Schopf, 1984: Kelvin wave-induced anomalous advection and the onset of surface warming in El Nino events. Mon. Wea. Rev., 112, 923-933.

Holland, G.J., 1986: Interannual variability of the Australian summer monsoon at Darwin: 1952-82. Mon. Wea. Rev., 114, 594-604.

Houze, R.A., S.G. Geotis, F.D. Marks and A.K. West, 1981: Winter monsoon convection in the vicinity of North Borneo. Part I: Structure and time variation of the clouds and precipitation. Mon. Wea. Rev., 109, 1596-1614.

Keen, R., 1982: The role of cross-equatorial cyclone pairs in the Southern Oscillation. Mon. Wea. Rev., 110, 1405-1416.

Krishnamurti, T.N., and H.N. Bhalme, 1976: Oscillations of a monsoon system. Part I: Observational aspects. J. Atmos. Sci., 33, 1937-1954.

_____, and D. Subrahmanyam, 1982: The 30-50 day mode at 850 mb during MONEX. J. Atmos. Sci., 39, 2088-2095.

Lau, K.-M., and P.H. Chan, 1985: Aspects of the 40-50 day oscillation during the northern winter as inferred from outgoing longwave radiation. Mon. Wea. Rev., 113, 1889-1909.

_____, and S.H. Shen, 1988: On the dynamics of intraseasonal oscillation and ENSO. J. Atmos. Sci., 45, in press.

Lim, H., and C.-P. Chang, 1981: A theory of midlatitude forcing of tropical motions during winter monsoons. J. Atmos. Sci., 38, 2377-2392.

Livezey, R.E., and W.Y. Chen, 1983: Statistical field significance and its determination by Monte Carlo techniques. Mon. Wea. Rev., 111, 46-59.

Lukas, R., S.P. Hayes and K. Wyrtki, 1984: Equatorial sea level response during the 1982-83 El Nino. J. Geophys. Res., 89, 10425-10430.

Luther, D.S., D.E. Harrison and R.A. Knox, 1983: Zonal winds in the central equatorial Pacific and El Nino. Science, 222, 327-330.

Madden, R.A., and P.R. Julian, 1972: Description of global scale circulation cells in the tropics with a 40-50 day period. J. Atmos. Sci., 29, 1109-1123.

McCreary, J.P., Jr., 1983: A model of tropical ocean-atmosphere interaction. Mon. Wea. Rev., 111, 370-387.

Meehl, G.A., 1987: The annual cycle and interannual variability in the tropical Pacific and Indian Ocean regions. Mon. Wea. Rev., 115, 27-50.

Mitchum, G.T., 1987: Trade wind fluctuations associated with El Nino-Southern Oscillation events. J. Geophys. Res., 92, 9464-9468.

Murakami, M., 1979: Large-scale aspects of deep convective activity over the GATE area. Mon. Wea. Rev., 107, 994-1013.

Murakami, T., 1987: Intraseasonal atmospheric teleconnection patterns during the Northern Hemisphere summer. Mon. Wea. Rev., 115, 2133-2154.

_____, 1988a: Intraseasonal atmospheric teleconnection patterns during the Northern Hemisphere winter. J. Climate, 1, 117-131.

_____, 1988b: Relationship between sea surface temperature and outgoing longwave radiation on intraseasonal time scales. Tenki, J. Meteor. Soc. Japan, 35, in press.

_____, and F.P. Ho., 1972: Spectrum analysis of cloudiness over the northern Pacific. J. Meteor. Soc. Japan, 50, 285-311.

_____, and T. Nakazawa, 1985: Tropical 45 day oscillations during the 1979 Northern Hemisphere summer. J. Atmos. Sci., 42, 1107-1122.

_____, L.-X. Chen and A. Xie, 1986: Relationship among seasonal cycles, low-frequency oscillations, and transient disturbances as revealed from outgoing longwave radiation data. Mon. Wea. Rev., 114, 1456-1465.

_____, and W.L. Sumathipala, 1988: Westerly bursts during the 1982/83 ENSO. J. Climate, 1, in press.

Nakazawa, T., 1988: Tropical supercluster within intraseasonal variation over the western Pacific. J. Meteor. Soc. Japan, 66, in press.

Panofsky, H.A., and G.W. Brier, 1958: Some Applications of Statistics to Meteorology, Pennsylvania State University, 219pp.

Rasmusson, E.M., and T.H. Carpenter, 1982; Variations in tropical sea surface temperature and surface wind fields associated with the Southern Oscillation/El Nino. Mon. Wea. Rev., 110, 354-384.

Reed, R.J., and E.E. Recker, 1971: Structure and properties of synoptic-scale wave disturbances in the equatorial western Pacific. J. Atmos. Sci., 28, 1117-1133.

Sumathipala, W.L., and T. Murakami, 1988: Intraseasonal fluctuations in low-level meridional winds over the south China Sea and the western Pacific and monsoonal convection over Indonesia and northern Australia. Tellus, 40A, 205-219.

Wallace, J.M., and C.-P. Chang, 1969: Spectrum analysis of large-scale wave disturbances in the tropical lower troposphere. J. Atmos. Sci., 26, 1010-1025.

Wang, X.-L., and T. Murakami, 1988: Intraseasonal disturbance activity before, during, and after the 1982/83 ENSO. J. Atmos. Sci., 45, in press.

Wyrtki, K., 1975: El Nino - the dynamic response of the equatorial Pacific Ocean to atmospheric forcing. J. Phys. Oceanogr., 15, 572-584.

Yamagata, T., 1988: A simple air-sea coupled model of the origin of intraseasonal and interannual disturbances in the tropics. Jacob Bjerknes Symposium on Air-Sea Interaction, February 1-5, 1988, Anaheim, California.

Yanai, M., T. Nitta and Y. Hayashi, 1968: Power spectra of large-scale disturbances over the tropical Pacific. J. Meteor. Soc. Japan, 46, 308-323.

Yasunari, T., 1980: A quasi-stationary appearance of 30-40 day period in the cloudiness fluctuations during the summer monsoon over India. J. Meteor. Soc., 58, 225-229.

_____, 1987: Global structure of the El Nino/Southern Oscillation. Part I: El Nino composites. J. Meteor. Soc. Japan, 65, 67-98.

_____, 1988: Global teleconnections associated with the Asian monsoon and the ENSO. Jacob Bjerknes Symposium on Air-Sea Interaction, February 1-5, 1988, Anaheim, California.

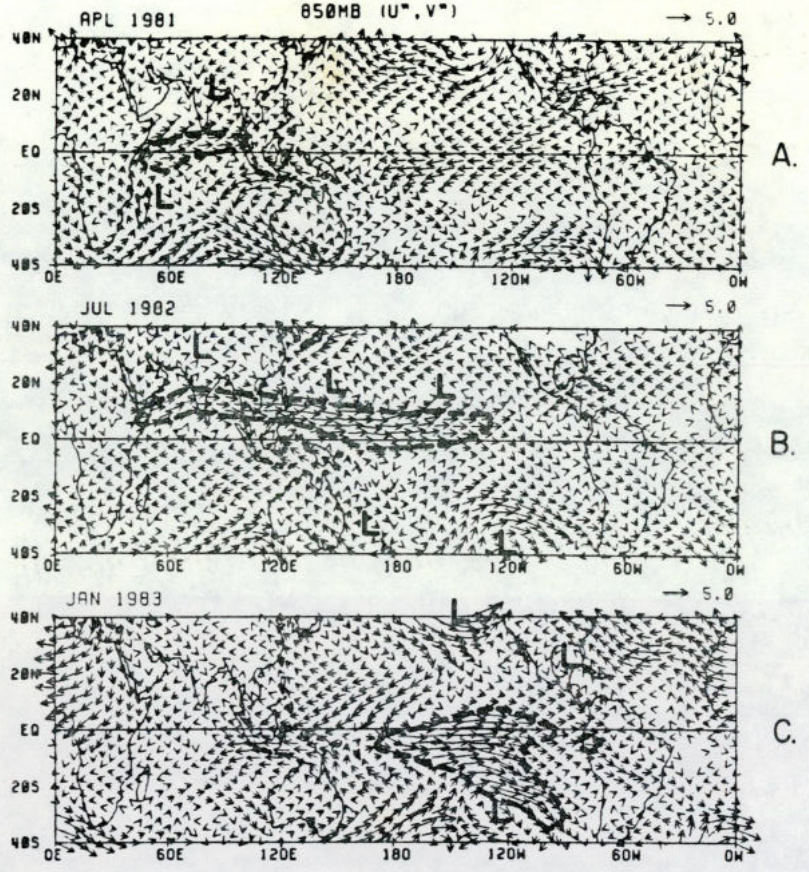

Fig. 2. 850 mb (u", v") winds (unit: 5 ms^{-1}) in (A) April 1981, (B) July 1982, and (C) January 1983. Heavy dashed lines indicate regions of westerlies greater than 5 ms^{-1}. Major cyclonic disturbances are indicated by "L".

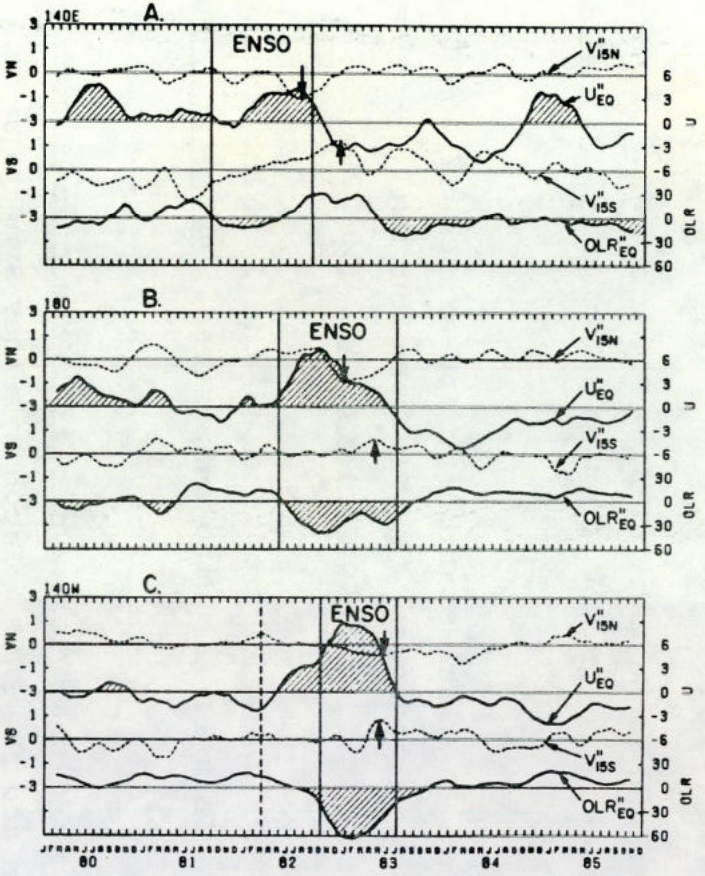

Fig. 1. Times series of u" (m s^{-1}) and OLR" (W m^{-2}) at the equator, as well as v" (m s-1) at 15°N and 15°S, respectively, during the 6 years of 1980-85. A : At 140°E, B : At 180°, C : At 140°W.

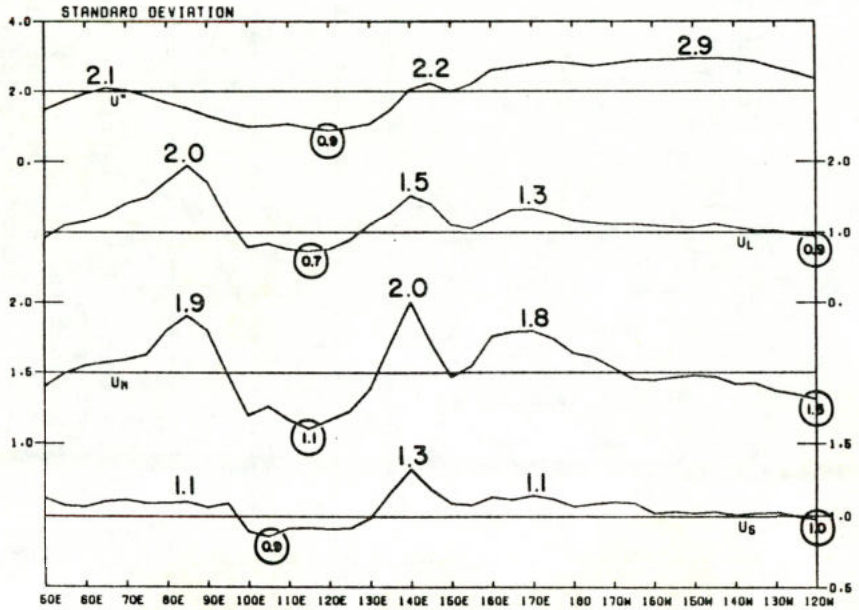

Fig. 4. Standard deviations (ms^{-1}) of u", u_L, u_M, and u_S at the equator from 50°E to 120°W during the 6 years of 1980-85.

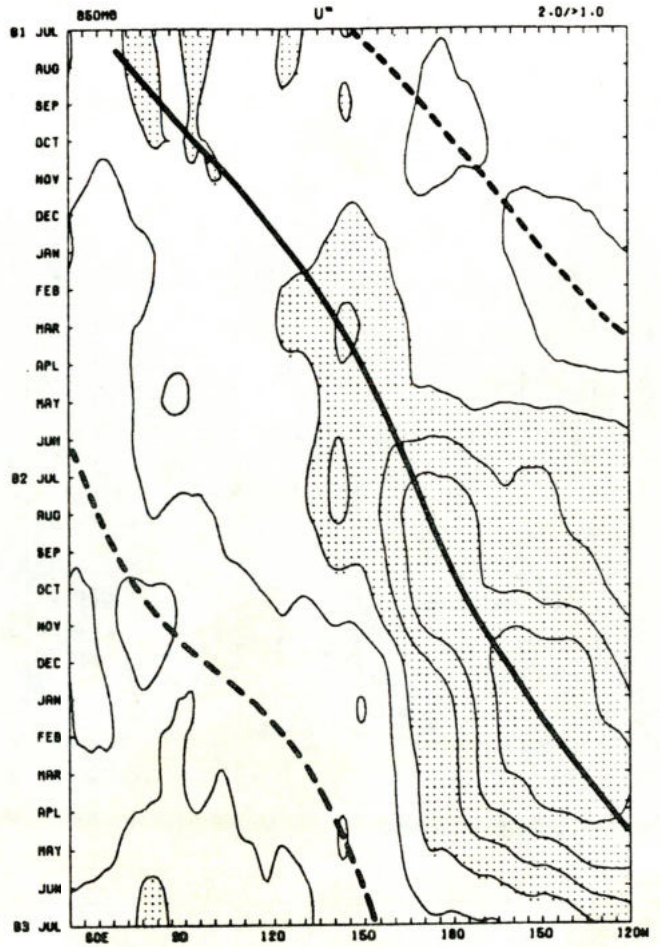

Fig. 3. 850 mb u" (interval: 2 ms^{-1}) at the equator. Shading indicates regions of westerly u" greater than +1 ms^{-1}. Heavy (dashed) lines indicate eastward propagation of westerly (easterly) u".

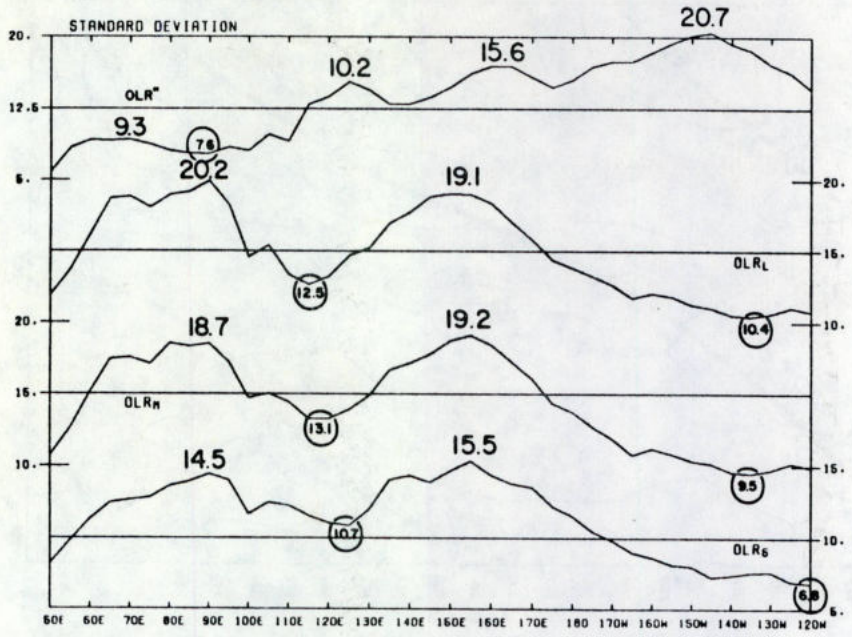

Fig. 5. As in Fig. 4, except for OLR", OLR_L, OLR_M, and OLR_S in units of W m^{-2}.

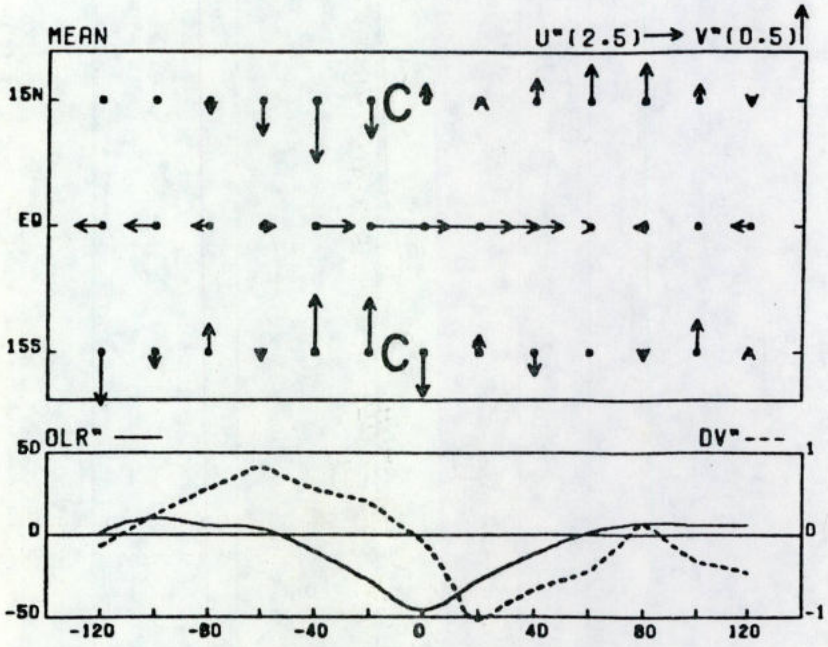

Fig. 6. Longitudinal distribution of mean u" (unit vector: 2.5 ms^{-1}), v" at 15°N and 15°S (unit vector: 0.5 ms^{-1}), OLR" (solid line: W m^{-2}), and divergence (dashed line: 10-6 s^{-1}). C denotes cyclonic center.

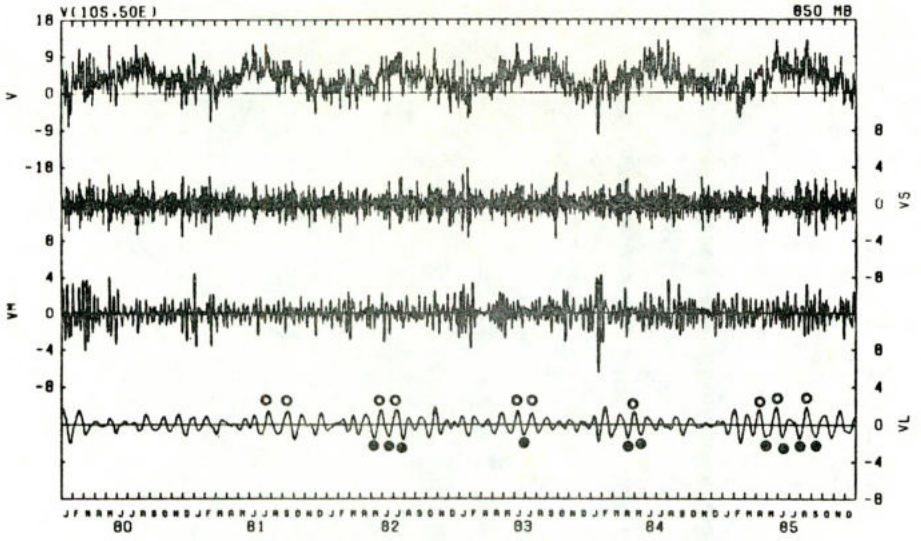

Fig. 7. Time series of daily v, v_S, v_M, and v_L at 850 mb over the Indian Ocean (10°S, 50°S) from 1980 to 85. Open circles (black dots) indicate strong southerly (northerly) v_L surges which were selected as the reference for the compositing in MJJASO.

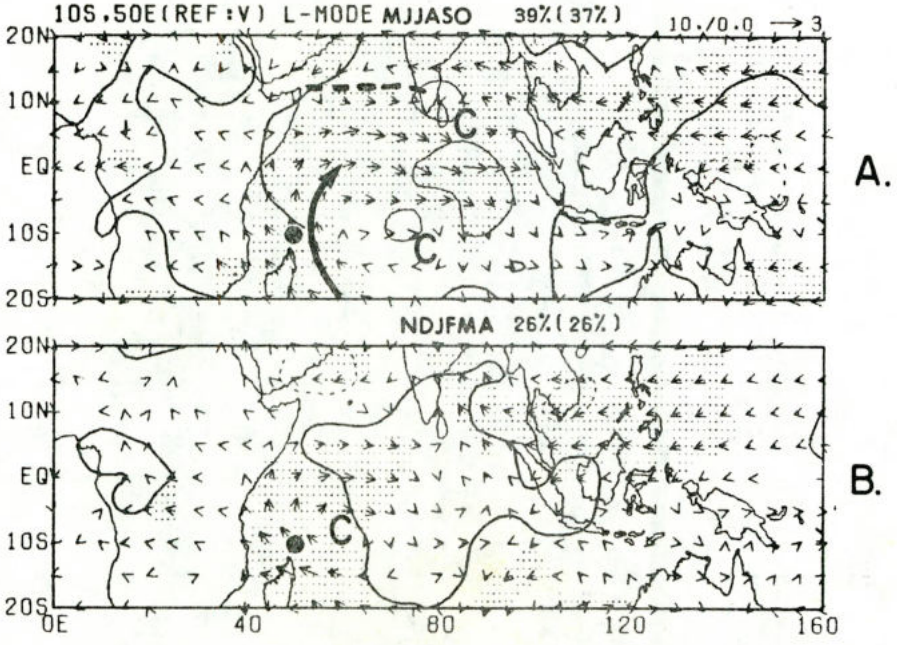

Fig. 8. Composite (u_L, v_L) wind fields at 850 mb in MJJASO (A) and NDJFMA (B) at the reference point (10°S, 50°E). Full lines represent OLR_L less than or equal to zero with interval of 10 W m^{-2}. Refer to text for further information.

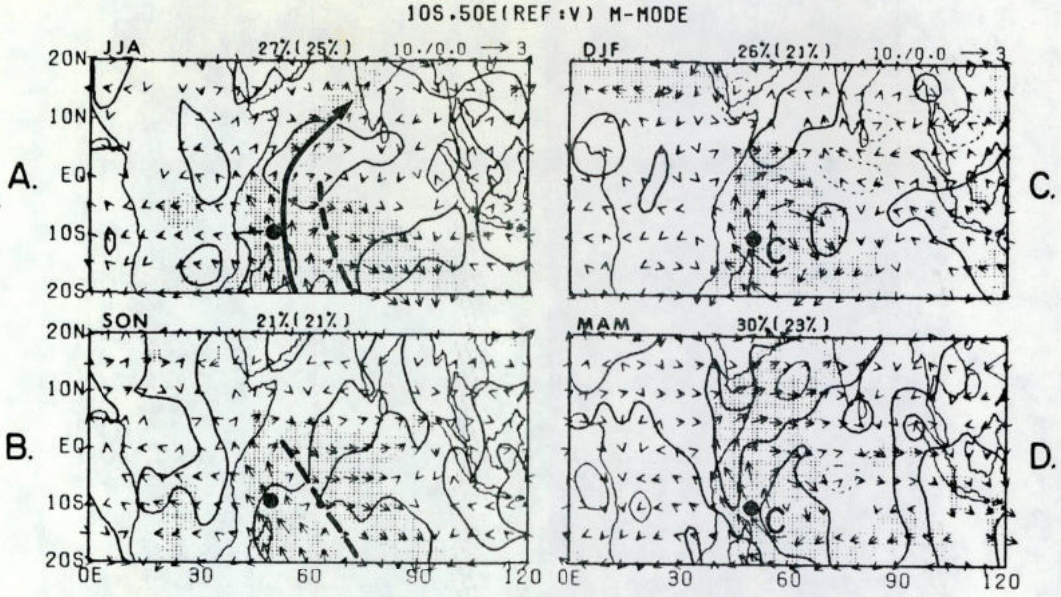

Fig. 9. Composite (u_M, v_M) wind fields for four seasons (JJA, SON, DJF, MAM) at the reference point (10°S, 50°E). Refer to Fig. 8 for further information.

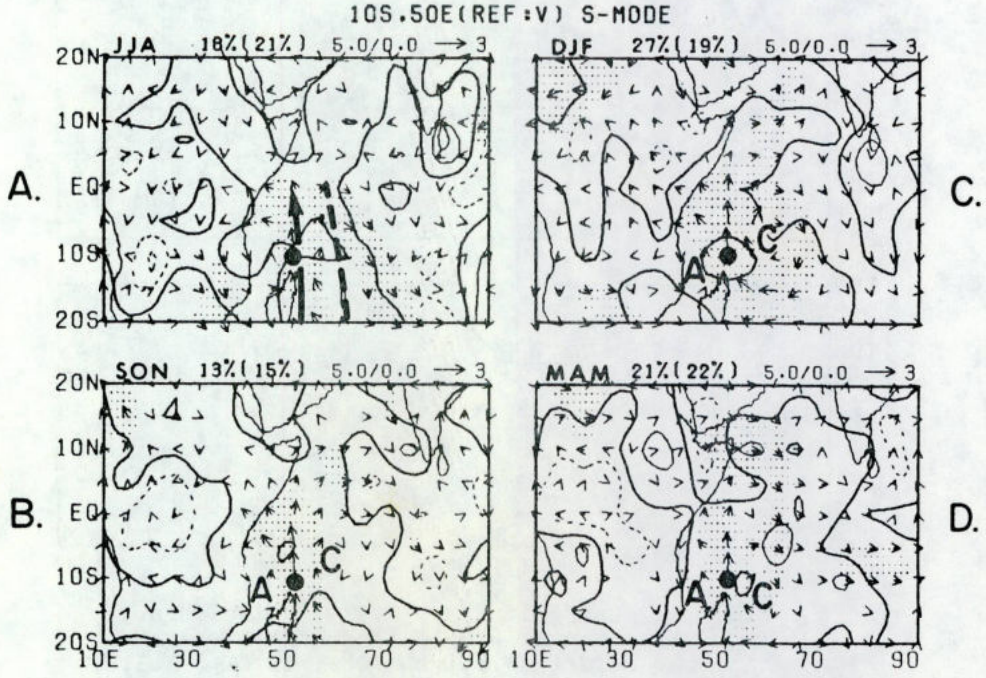

Fig. 10. As in Fig. 9, except for (u_S, v_S) wind fields.

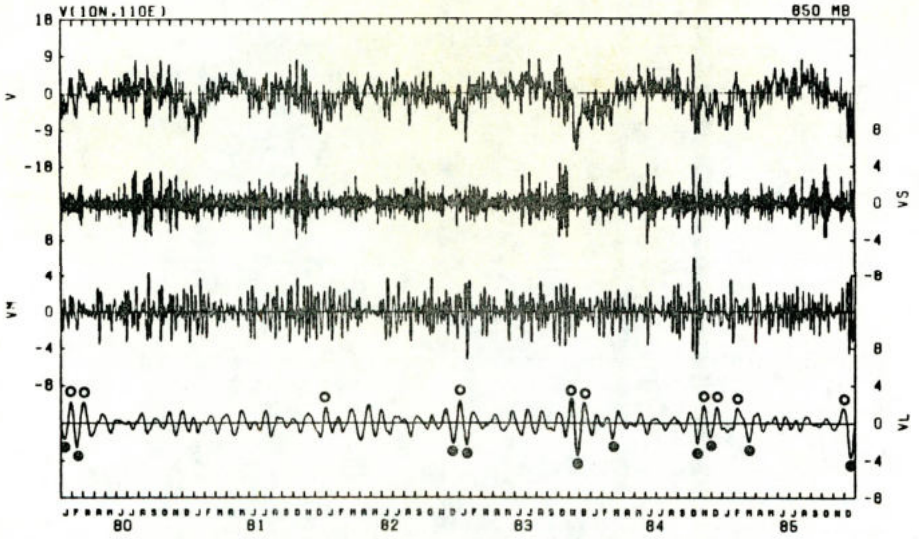

Fig. 11. As in Fig. 7, except for the reference point (10°N, 110°E).

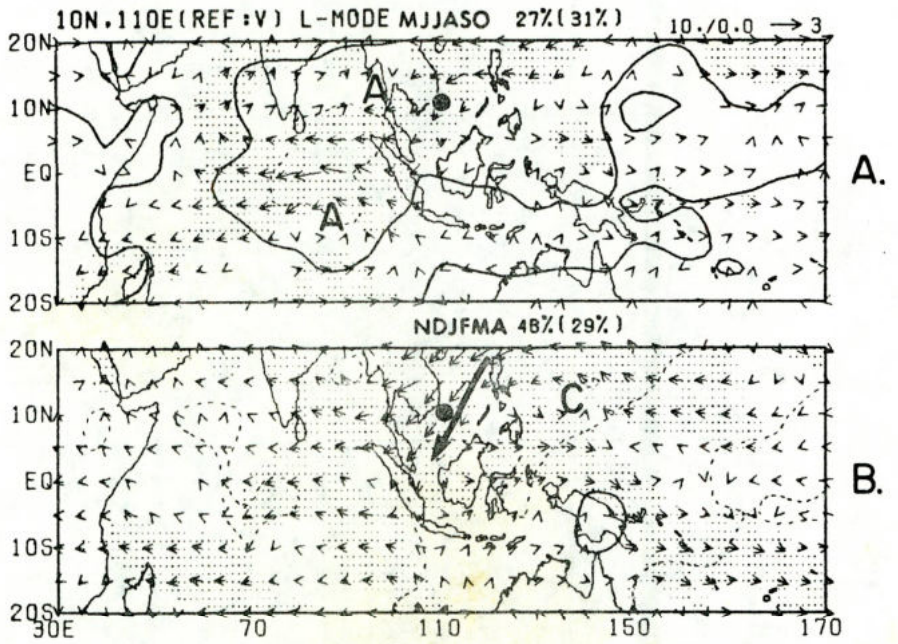

Fig. 12. As in Fig. 8, except for the reference point (10°N, 110°E).

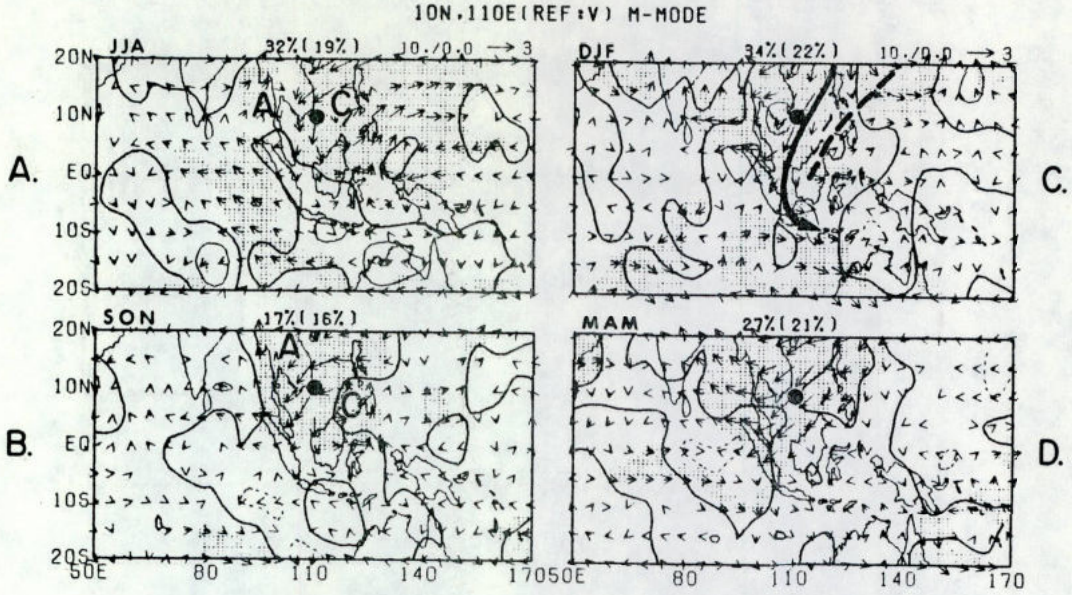

Fig. 13. As in Fig. 9, except for the reference point (10°N, 110°E).

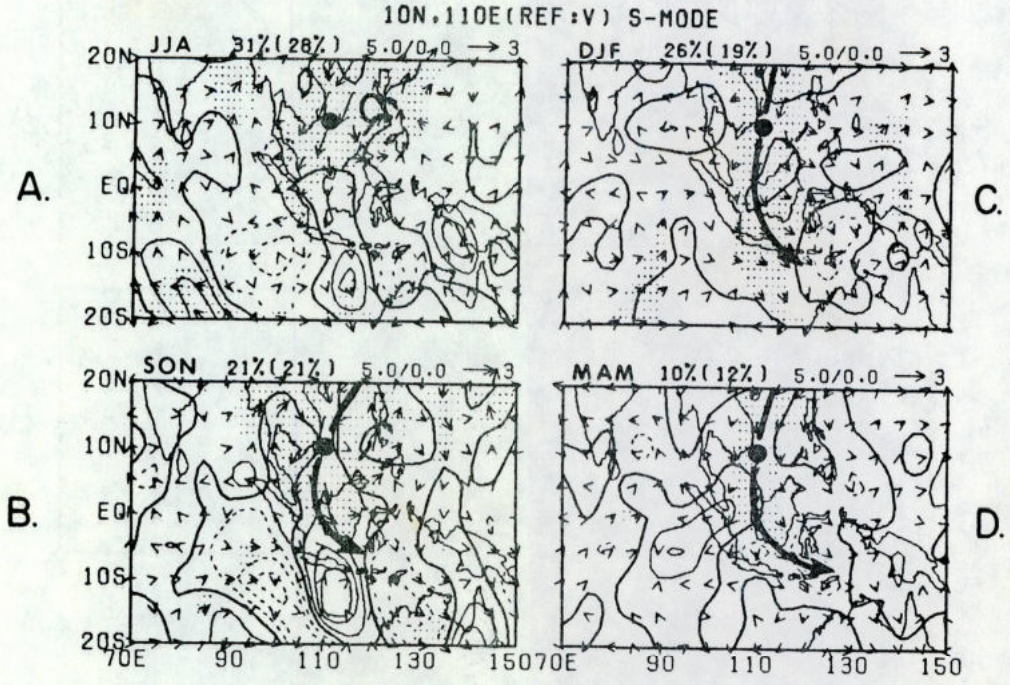

Fig. 14. As in Fig. 10, except for the reference point (10°N, 110°E).

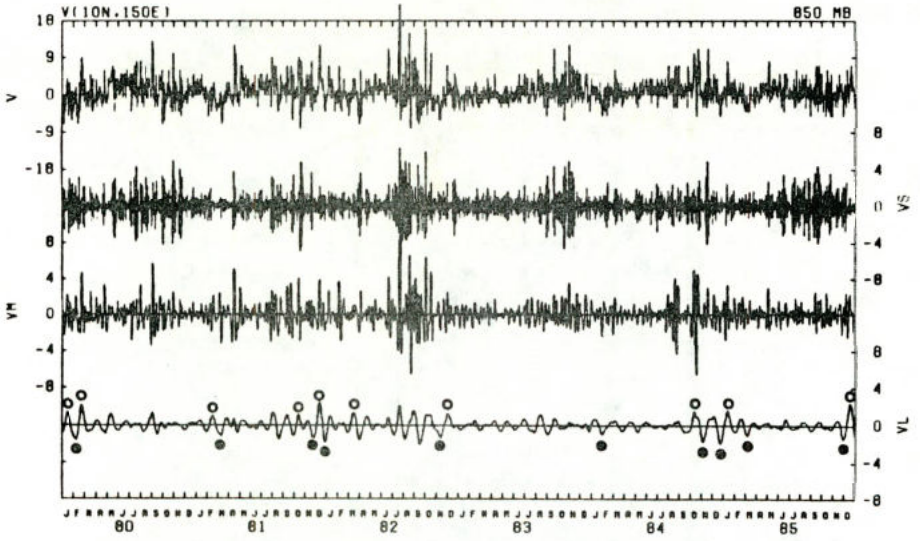

Fig. 15. As in Fig. 7, except for the reference point (10°N, 150°E).

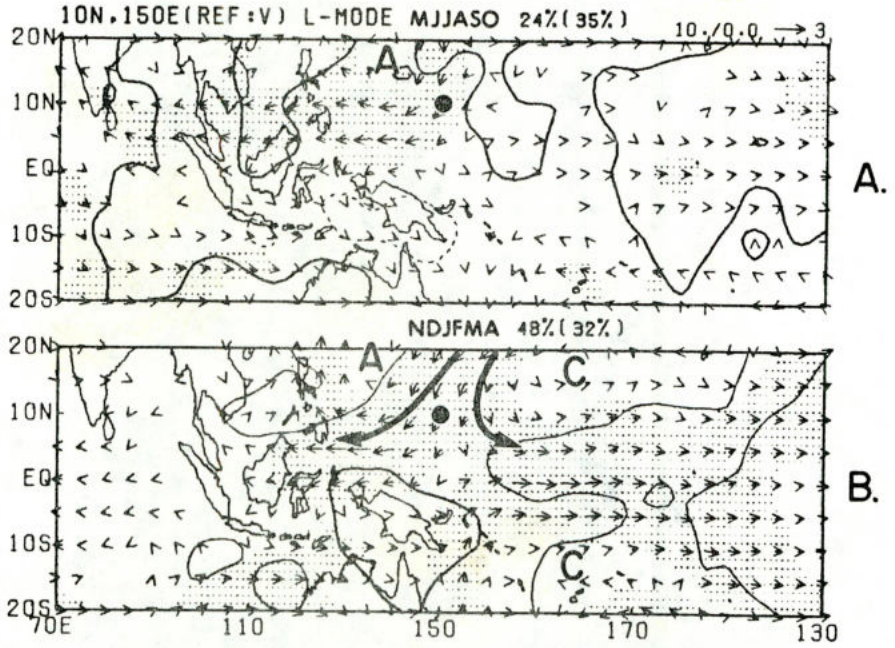

Fig. 16. As in Fig. 8, except for the reference point (10°N, 150°E).

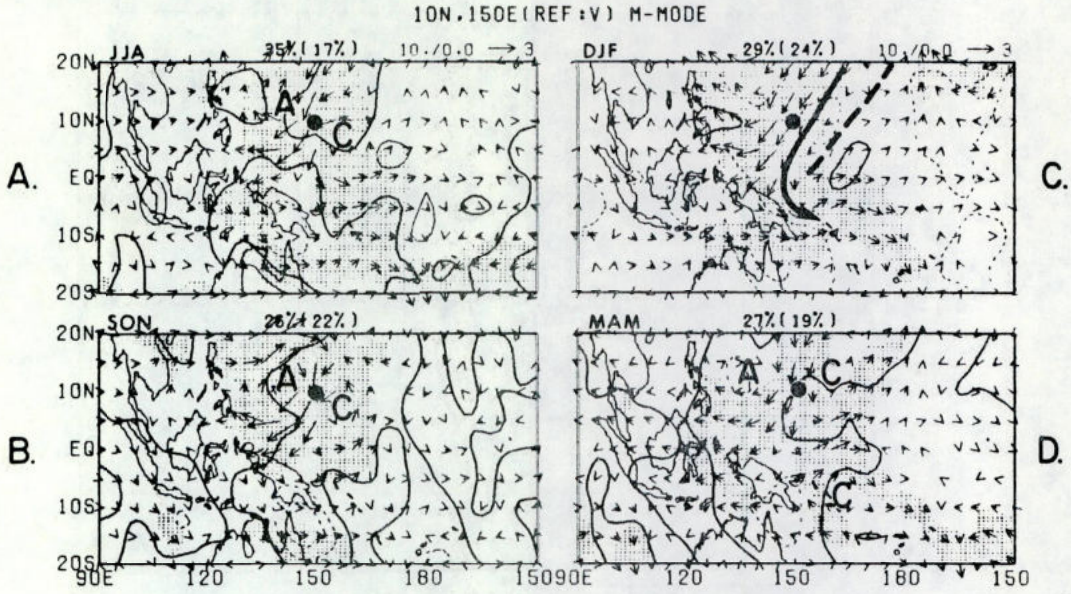

Fig. 17. As in Fig. 9, except for the reference point (10°N, 150°E).

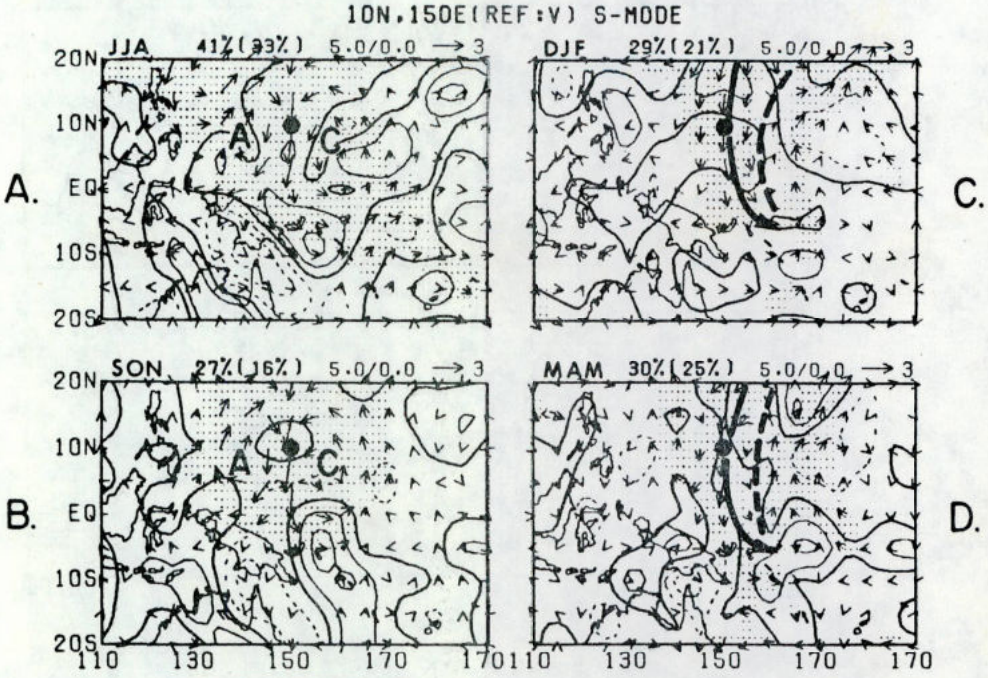

Fig. 18. As in Fig. 10, except for the reference point (10°N, 150°E).

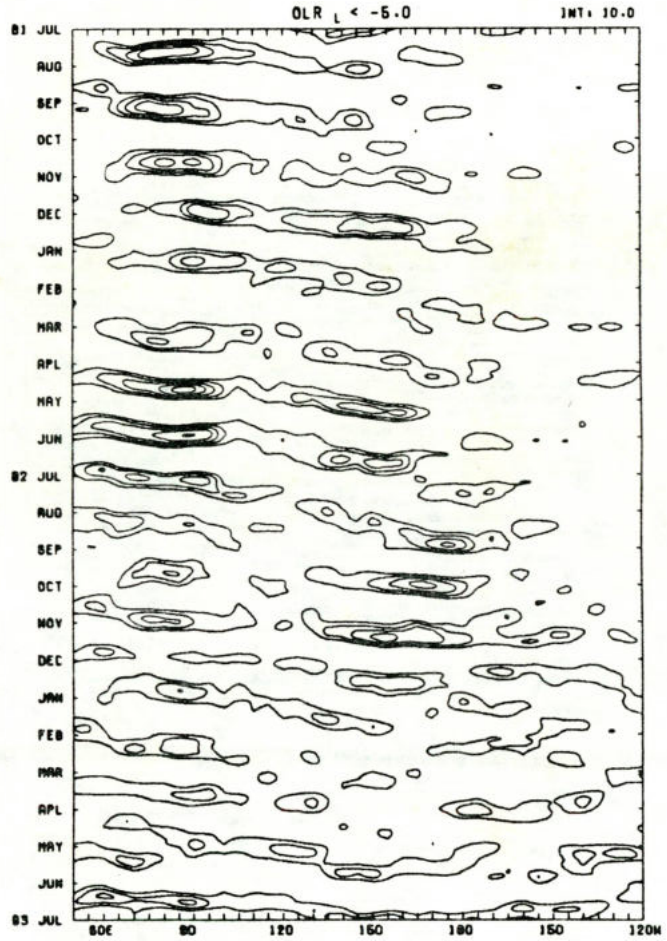

Fig. 20. Longitude-time section of negative OLR_L perturbations less than -5 W m^{-2}. Intervals are for 10 W m^{-2} (no zero and/or positive isolines).

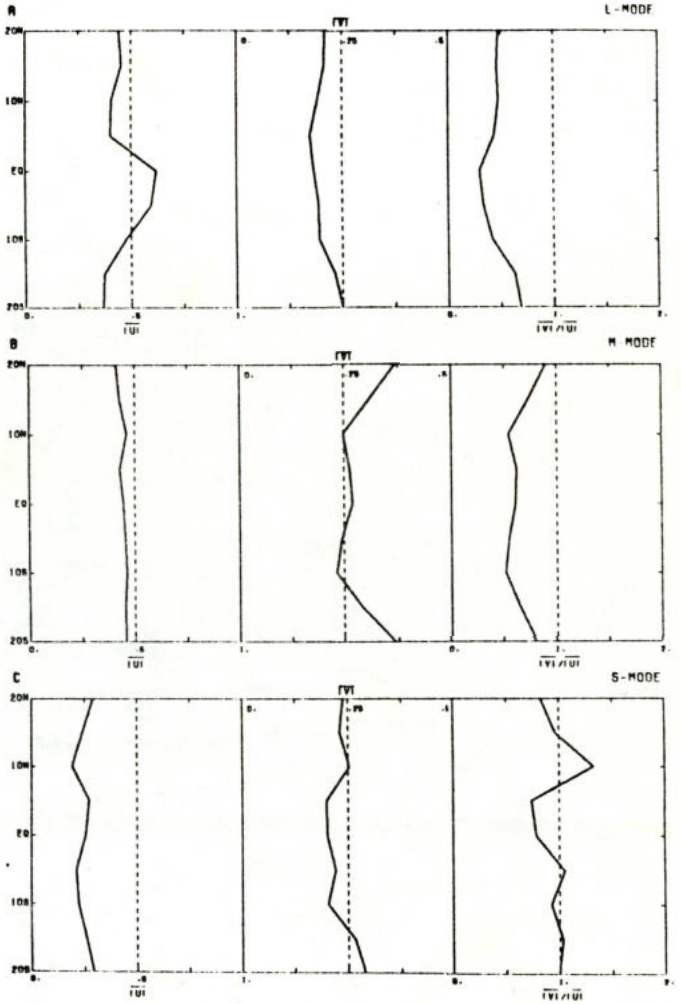

Fig. 19. Zonal mean $\overline{|u|}$, zonal mean $\overline{|v|}$, and the ratio $\overline{|v|}/\overline{|u|}$ for (A) L-mode, (B) M-mode, and (C) S-mode.

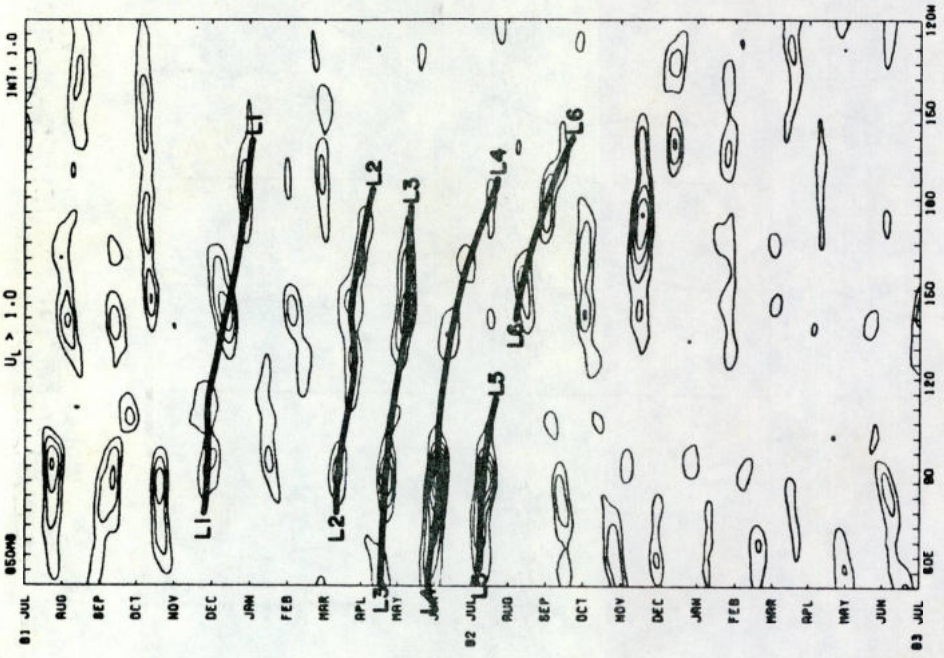

Fig. 21. Longitude-time section of positive (westerly) u_L perturbations greater than +1 ms^{-1}. Intervals are for 1 ms^{-1} (no zero and/or negative isolines). Major eastward propagating perturbations are shown by "L1", "L2", ..., and "L6".

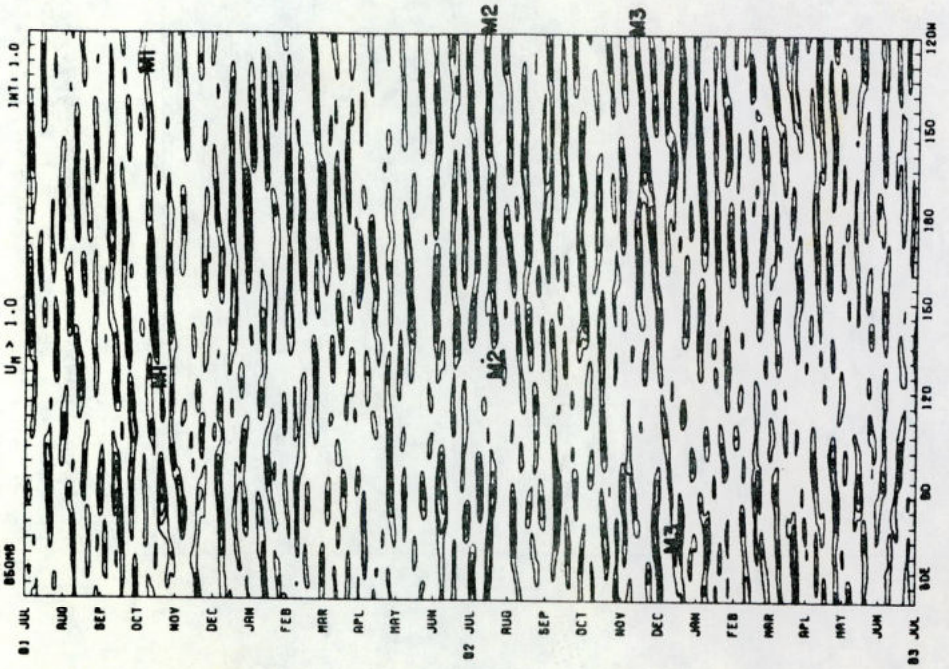

Fig. 22. As in Fig. 21, except for positive (westerly) u_M perturbations greater than +1 ms^{-1}. Typical westward propagating u_M perturbations are exemplified by M1, M2, and M3.

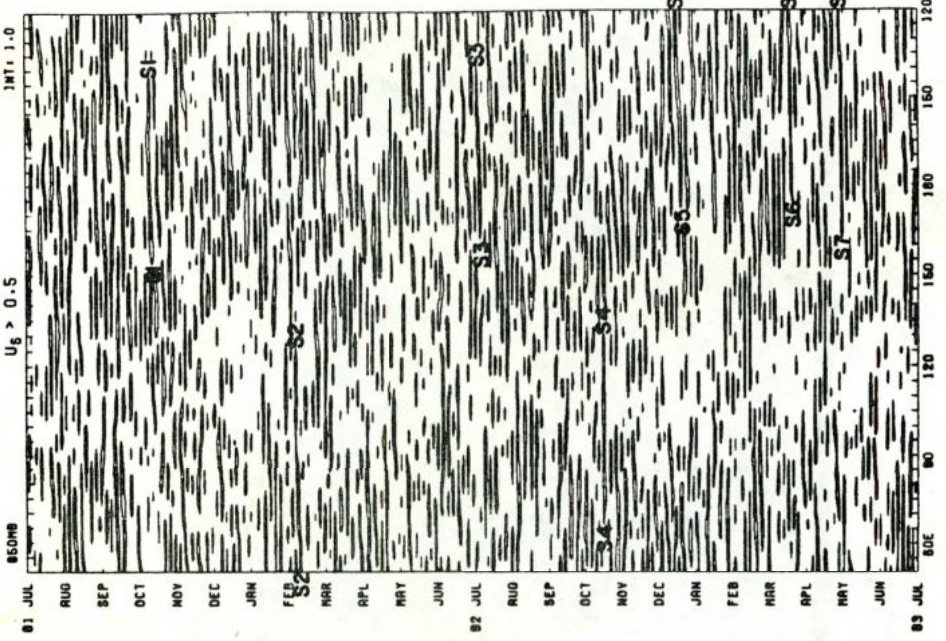

Fig. 23. As in Fig. 21, except for positive (westerly) u_S perturbations greater than +0.5 ms^{-1}. Examples of westward propagating u_S perturbations are shown by S1, S2, ..., and S7.

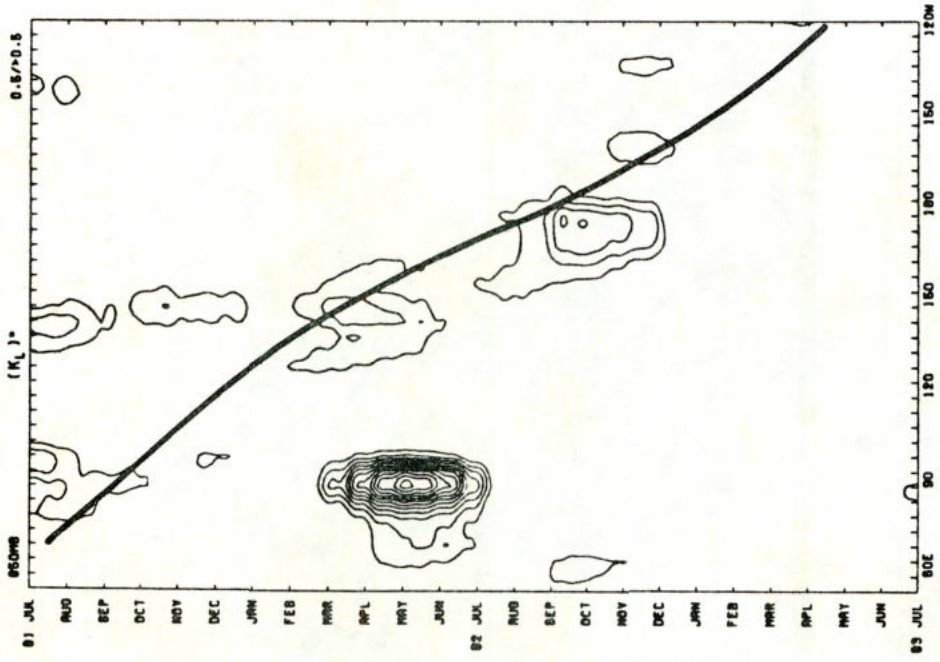

Fig. 24. Longitude-time section of $(K_L)''$ anomalies greater than +0.5 m^{2}s^{-2} (interval 0.5 m^{2}s^{-2}). Heavy full line indicates an eastward propagation of westerly u" perturbations (see Fig. 3).

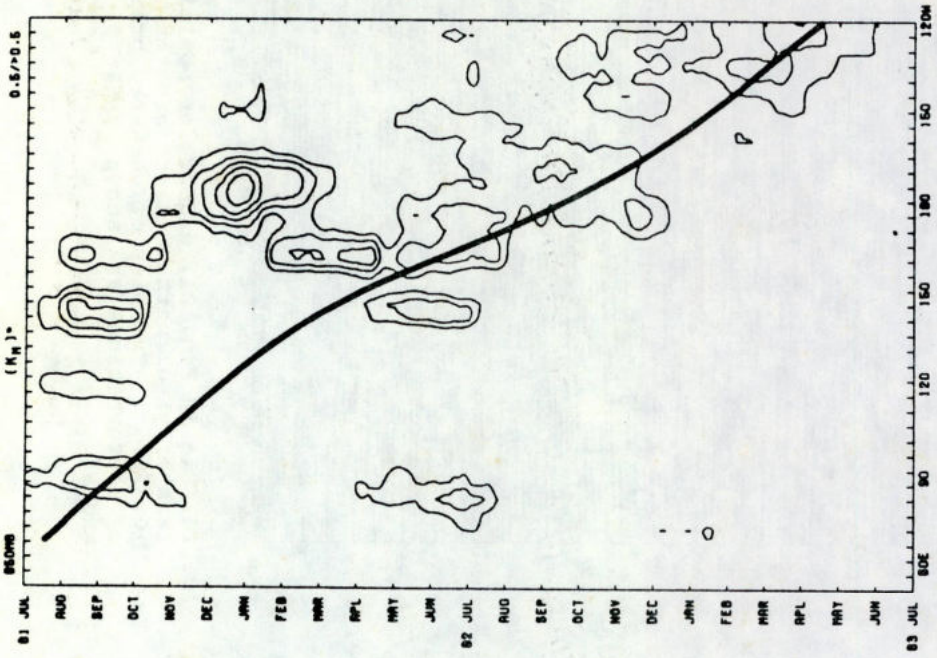

Fig. 25. As in Fig. 24, except for (K_M)".

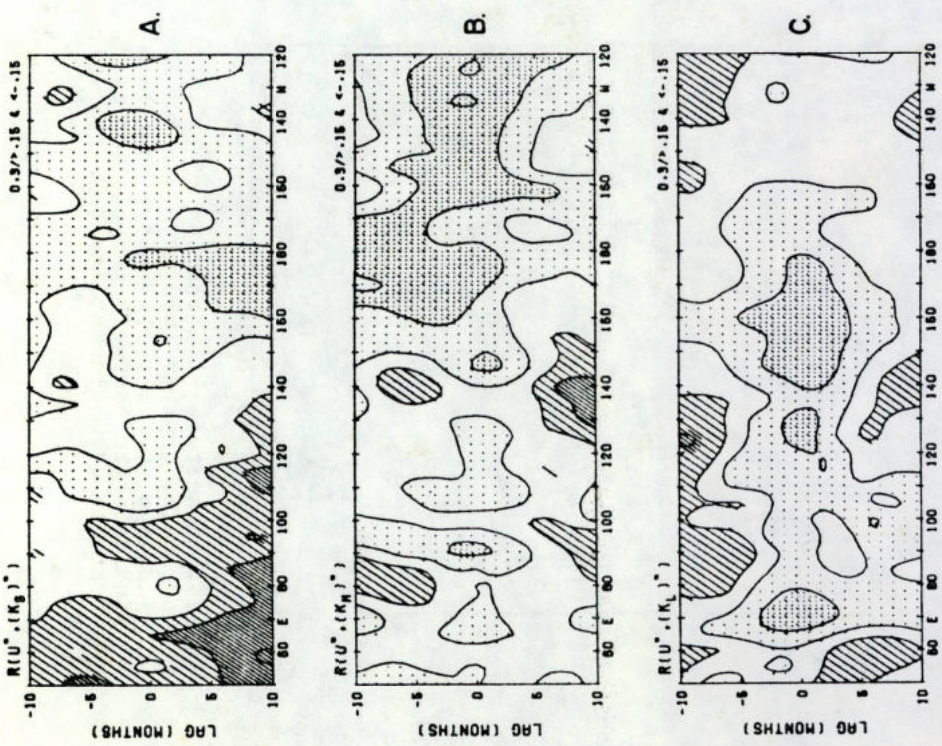

Fig. 26. A: Lag correlation between u" and (K_S)" at the equator from 50°E to 120°W. The ordinate is for lag months, e.g., +10 means (K_S)" lagging u" by 10 months. B: For (K_M)". C: For (K_L)". Intervals are 0.3. Shading (dark shading) indicates regions of negative correlation less than -0.15 (-0.45). Hatching (dark hatching) is for positive correlation greater than +0.15 (+0.45).